Linear and Non-Linear Perturbation Equations with Relaxation Source Terms for Forced Eddy Simulation of Aeroacoustic Sound Generation

R. Ewert[*], J. Dierke[†], A. Neifeld[‡]

Institute of Aerodynamics and Flow Technology, Technical Acoustics

Lilienthalplatz 7, 381208 Braunschweig, Germany

German Aerospace Center (DLR)

S.M. Alavi Moghadam[§]

Institute of Aerodynamics, RWTH Aachen

Wüllnerstr 5a, 52062 Aachen, Germany

Turbulence related sound is generated by the dynamics of fluctuating vorticity. For example, trailing edge noise is caused by vorticity traveling past the trailing edge. To excite fluctuating vorticity by forcing the linearized Euler equations (LEE) with right-hand side source terms, one peculiar problem is observable: while the rise of vorticity levels by external sources poses no problem, to properly lower them, the right-hand side terms must act as a sink, being exactly in anti-phase to the vorticity levels as present in the LEE solution. However, the accurate prediction of vorticity in terms of phase cannot be guaranteed, especially for approximately modeled sources e.g. using stochastic methods. Thus in general there will be a mismatch between actual induced and intended levels of vorticity. In this paper a new class of relaxation source terms is introduced that enables the proper excitation of vorticity levels in linear and non-linear perturbation equations and as such enables an accurate control over the vorticity magnitudes. The source can be formulated to act selectively in wave-number space, i.e. without directly affecting the dynamics of resolved low wave-number vorticity components whereas the resolved high wave-number part is piloted by the fluctuating vorticity imposed as a reference solution. The reformulation of the Navier-Stokes equations in primitive variables and non-linear perturbation form is presented. Direct noise computation of sound radiated from a vortex shedding cylinder in laminar cross flow verify their implementation. The relaxation source term without forcing is applied to the unstable jet problem of the 4th CAA Workshop on Benchmark Problems. The forcing of frozen and decaying stochastic turbulence in conjunction with the relaxation source term is studied. First results for high-lift noise prediction with forced eddy simulation are presented.

I.   Introduction

In Computational Aeroacoustics (CAA) the linearized Euler equations (LEE) are often adopted as linear governing equations which, however, exhibit some principle problems if augmented by right-hand side vortex sound source terms.

Firstly, these source terms in general act both as a direct acoustic source as well as a source of fluctuating vorticity. Fluctuating vorticity is essential for the proper simulation of airframe born noise mechanism based on the interaction of turbulence (vorticity) with surface irregularities (such as wing trailing edges). It might be observed that the onset of vorticity in the LEE is realized as desired by the source terms. However, the

---

[*]Senior Scientist, Senior Member AIAA, Corresponding Author roland.ewert@dlr.de.
[†]Research Scientist, Member AIAA.
[‡]Research Scientist, Member AIAA.
[§]Research Scientist.

American Institute of Aeronautics and Astronautics

removal of vorticity from the LEE (which include a vorticity transport mode) can only work if the right-hand side acts also as an exact anti-phase sink term. Hence, a fluctuating source term that provides quantitative correct levels of amplitude but otherwise lacks a proper sink quality is insufficient as it eventually will cause wrong levels of vorticity in the LEE solution.

Secondly, the LEE describe hydrodynamic instabilities that are not restricted in amplitude by non-linear terms. One way to avoid this problem is to use fully non-linear perturbation equations with viscous terms. However, inclusion of the non-linear terms on the left-hand side effectively means to move them from the right-hand side, where they initially represented the actual source terms. This rises the question how to properly formulate source terms for non-linear perturbation equations.

In previous work Acoustic Perturbation Equations (APE) have been proposed,[1] which, by shifting linear terms of the LEE to the right-hand side (i.e. imposing them as external sources), i) are not prone to hydrodynamic instabilities any more (disabling the vorticity transport property of the LEE while keeping the degree of freedom to resolve vorticity fluctuations) and ii) realize the control of vorticity transport entirely by the resulting right-hand side source terms. With this approach airframe noise prediction capability has been successfully demonstrated in various publications e.g. modeling the right-hand side sources with stochastic methods. The essential feature of this approach is that the complete vortex dynamics are imposed by the external source terms (we will subsequently refer to this approach as deterministic noise source model). This is highly advantageous if the sources have been produced by precursor scale resolving simulations which include the entire vortex dynamics.

Especially with the use of stochastic sound sources it would be desirable to extend the approach to have a selective spectral source term, that affects only the high wave-number part, whereas vortex dynamics especially in the low wave-number regime well resolved on the CAA mesh are simulated directly. This way it would become feasible to bridge the simulation gap between fully deterministic noise source modeling and direct noise computation where all turbulent dynamics are completely resolved. A similar goal is aimed at in Coherent Vortex Simulation (CVS).[2–4] It implies that governing equations utilized represent the non-linear Navier-Stokes equations. A non-linear acoustic solver (NLAS) forced by stochastic sources has been proposed by Batten el al.[5]

In this work we introduce a new class of right-hand side forcing terms, which are formulated as relaxation source terms based on fluctuating vorticity. Due to the formulation as a relaxation source term, the desired sink-term quality is obtained. In this regard, it is important that the source term acts exclusively on the vorticity mode and does not generate undue additional spurious noise. We present formulations that can be used in conjunction with linear as well as non-linear perturbation equations. The source terms can be formulated to act 'artificially selective' in wave-number space, i.e. without directly affecting the dynamics of resolved low wave-number components. To be precise, only the high wave number part of the resolved fluctuating vorticity would be 'piloted' according to the reference vorticity fluctuations used in the relaxation source term. If the fluctuating vorticity exhibits a spectral sharp wave-number cut-off for large wave numbers it can realize both, the removal of small vorticity structures beyond the cut-off and providing the backscatter of energy into the resolved spectrum.

We demonstrate that by prescribing zero target vorticity, hydrodynamic instabilities can be removed from the linearized Euler equations. The future goal of this research aims at bridging the gap between a fully deterministic sound source model based on stochastic sources from the Fast Random particle-Mesh method (FRPM[6–8]), towards fully scale resolving simulation without any additional modeling. Partly scale resolving simulation in principle allows to capture flow-acoustic feedback mechanism (e.g. Rossiter modes) otherwise not present in fully deterministic sound source models.

In Section II the relaxation source term is introduced and some of its features are studied theoretically. In Section III we present the derivation of the Navier-Stokes equations as non-linear perturbation equations over an (arbitrary) mean flow. In Section IV numerical results are shown, starting with results of a direct numerical simulation of noise radiated from a circular cylinder in laminar cross-flow. Next, three test cases are presented demonstrating the application of the relaxation term. First, the relaxation source term without forcing is applied to the unstable jet problem of the 4th CAA Workshop on Benchmark Problems.[9] Next, the forcing with frozen and decaying stochastic turbulence in conjunction with the relaxation source term is studied. Finally, first results for high-lift noise prediction with forced eddy simulation are presented. The results are summarized in Section V.

American Institute of Aeronautics and Astronautics

(a) APE with linear Lamb vector source.
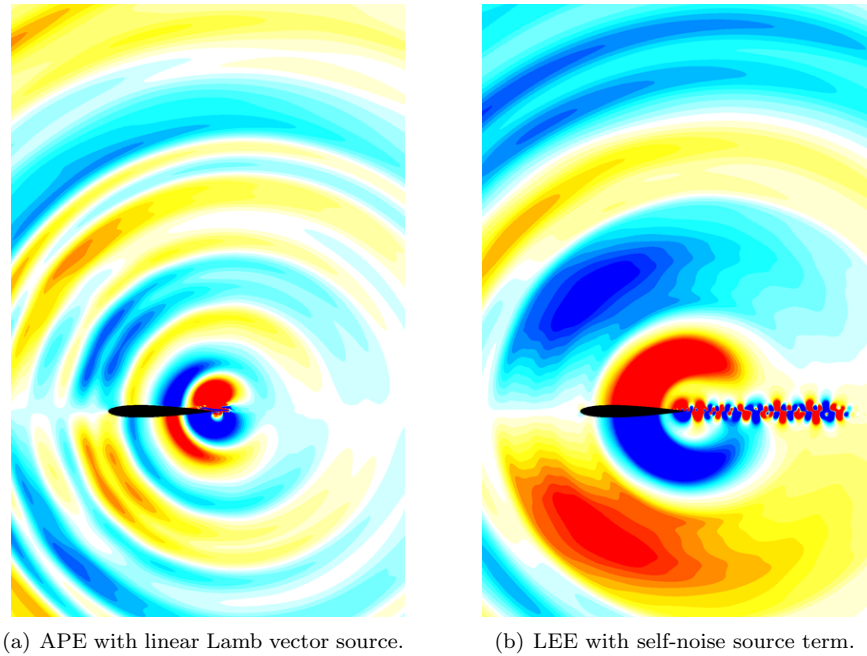
(b) LEE with self-noise source term.

Figure 1. Sound radiation from a NACA 0012 airfoil with externally imposed sound sources derived from the same stochastic realization of synthetic turbulence (fluctuating velocity).

II.   Relaxation sources for the LEE

A.   LEE with standard self-noise source term

Figure 1 shows CAA results obtained with linear perturbation equations forced by external source terms for trailing edge noise generated at a NACA0012 airfoil. The underlying stochastic fluctuating velocity model used to prescribe the right-hand side sources is the same for both cases. Figure 1(a) presents results using Acoustic Perturbation Equations, Ref.[10] and figure 1(b) gives results for the same flow case using the linearized Euler equations with evaluated self-noise source term. In both cases the turbulent sources are spatially weighted to restrict their effect right to the vicinity of the trailing edge $(0.8 < x/c < 1.2)$ and to smoothly ramp the sources up and down. Since the APE support no vortex convection, no vorticity is present outside the source region. In case of the LEE large amount of vorticity is convected out off the source region, becoming visible as a wake downstream of the airfoil, i.e. although the vorticity in the forcing source reduces to zero, this is not the case in the LEE simulation. Furthermore, the acoustic levels are slightly increased in the LEE simulation, indicating effectively too high levels of vorticity at the trailing edge. In the present simulation the downstream wake has no further effect on the radiated aeroacoustics. However, for more complex problems where additional downstream obstacles are present, the excited wake would create additional sound.

B.   LEE with new relaxation source term

The proper formulation of a relaxation source term for the wave-number selective forcing of fluctuating vorticity in perturbation equations is discussed next for the linearized Euler equations (LEE), where the term occurs as an additional source on the right-hand side of the perturbed momentum equation. However, the relaxation source term is also applicable in the same manner as a right-hand side source of general non-linear perturbation equations. In Section III the reformulation of the Navier-Stokes equations in terms of primitive perturbations over a steady (Favre-averaged) RANS mean-flow is presented. For the simulation of aeroacoustic sound propagation often the LEE are adopted which follow from the more general system

American Institute of Aeronautics and Astronautics

Eqs. (52-54) by neglecting heat-flux and fluctuating viscous stresses and neglecting non-linear terms, viz.

$$\frac{\partial \rho'}{\partial t} + \frac{\partial}{\partial x_i} \left(\rho' v_i^0 + \rho^0 v_i' \right) = 0 \tag{1}$$

$$\frac{\partial v_i'}{\partial t} + v_j^0 \frac{\partial v_i'}{\partial x_j} + v_j' \frac{\partial v_i^0}{\partial x_j} + \frac{\rho'}{\rho^0} v_j^0 \frac{\partial v_i^0}{\partial x_j} + \frac{1}{\rho^0} \frac{\partial p'}{\partial x_i} = -\epsilon_{ijk} \frac{\partial}{\partial x_j} \left[\sigma \left(\Omega_k' - \Omega_k^{ref} \right) \right] \tag{2}$$

$$\frac{\partial p'}{\partial t} + v_i^0 \frac{\partial p'}{\partial x_i} + v_i' \frac{\partial p^0}{\partial x_i} + \gamma p^0 \frac{\partial v_i'}{\partial x_i} + \gamma p' \frac{\partial v_i^0}{\partial x_i} = 0. \tag{3}$$

Note, although the system is termed 'linearized Euler equations', the mean-flow includes the effect of viscosity and heat conductivity (i.e. must not be a time-averaged Euler flow). The derivation of the right-hand side relaxation term in Eq. (2) and some of its theoretical features are discussed in the next paragraphs.

C.   Vorticity selective relaxation source

The goal of this paper is the formulation of a relaxation source term that satisfies the following constraints:

1. enable the excitation and proper control of fluctuating vorticity of linear and non-linear perturbation equations in a specified limited spatial domain,

2. leave other wave modes, especially acoustic waves, unaffected even if high levels of vorticity are manipulated,

3. support a wave-number selective forcing in order to enable partly scale resolved simulation, i.e. the low wave-numbers are unforced and their dynamics are a entirely prescribed by the governing equations (including the back scattering effect of higher wave-numbers), whereas higher wave-numbers are prescribed according to the reference solution.

In previous work by Freund[11] an aeroacoustic relaxation source has been proposed for the simulation of jet noise. In this model the fluctuating density from direct numerical simulation is imposed on the right-hand side of an acoustic equation system equivalent to the wave equation in steady flow,

$$\frac{\partial \rho}{\partial t} + \frac{\partial v_j}{\partial x_j} = -\sigma \left(\rho - \rho^{ref} \right) \tag{4}$$

$$\frac{\partial v_i}{\partial t} + a_\infty^2 \frac{\partial \rho}{\partial x_i} = 0, \tag{5}$$

where a_∞ is the sound speed, ρ is the density, p is the pressure, v_i the velocity, and σ a relaxation parameter specified for a source region with limited spatial extension. The density ρ^{ref} indicates an unsteady solution to the density fluctuations inside the source region defined by the extension of σ. The right-hand side source works akin to a PID controller: if the target density ρ deviates from its reference ρ^{ref}, the right-hand side source forces the solution towards the reference. The control stiffness is defined by the magnitude of parameter σ. The first order system above can be recast into a simple wave equation and it was shown by Freund[11] that if ρ^{ref} represents a solution to the Navier-Stokes equations the resulting right-hand side relaxation source becomes equivalent up to order $O(\sigma^{-1}, \omega^3)$ (where ω denotes angular frequency) to the source term of the Lighthill acoustic analogy $\partial^2 T_{ij}/\partial x_i \partial x_j$, $T_{ij} = \rho v_i v_j + \left(p - a_\infty^2 \rho \right) \delta_{ij} - \tau_{ij}$. Hence, convergence to Lighthill's acoustic analogy[12] is obtained for a value of the relaxation parameter being sufficiently large.

If the relaxation term is defined for a buffer zone at the boundary of the computational domain for all dependent flow variables, a sponge layer boundary condition is obtained that damps out outgoing waves and allows with a properly prescribed reference solution the simultaneous excitation of incoming waves.

To put forward a vorticity based relaxation, it is essential to use the difference of actual fluctuating vorticity (indicated by a prime),

$$\Omega_i' = \epsilon_{ijk} \frac{\partial v_k'}{\partial x_j}, \tag{6}$$

and an externally imposed fluctuating reference vorticity, i.e. $\Omega'_i - \Omega_i^{ref}$, as the main key parameter. Furthermore, to only excite vorticity fluctuations and to not affect acoustic modes, the forcing function must be expressed as the curl of a vector function $\nabla \times \boldsymbol{f}$ on the right-hand side of the momentum equation (which is a consequence of the discussion e.g. put forward in Ref.[1]), or, written in tensor notation

$$\frac{\partial v'_i}{\partial t} + \cdots = \epsilon_{ijk} \frac{\partial f_k}{\partial x_j} \tag{7}$$

The simplest vector function possible is the fluctuating vorticity difference times a proportionality constant. The corresponding relaxation source reads

$$\frac{\partial v'_i}{\partial t} + \cdots = -\epsilon_{ijk} \frac{\partial}{\partial x_j} \left[\sigma \left(\Omega'_k - \Omega_k^{ref} \right) \right], \tag{8}$$

where σ specifies the relaxation control parameter, which is a function of spatial coordinate, and Ω'_i is the vorticity that derives by means of Eq. (6) from the left-hand side fluctuating velocity.

D. Relaxation term toy model

To discuss further the properties of the relaxation term in Eq. (8), we assume the simplified 2-D problem of a uniform mean-flow in x-direction ($v_1^0 = const.$, $v_2^0 = 0$) with constant relaxation parameter ($\sigma = const.$) and consider the momentum equation of the linearized Euler equations (LEE). Taking the curl of the momentum equation, the fluctuating vorticity equation with right-hand side source term is obtained, which for the component 3 normal to the 2-D plane reads

$$\frac{\partial \Omega'_3}{\partial t} + v_1^0 \frac{\partial \Omega'_3}{\partial x_1} = \sigma \left(\frac{\partial^2 \Omega'_3}{\partial x_i^2} - \frac{\partial^2 \Omega_3^{ref}}{\partial x_i^2} \right). \tag{9}$$

To arrive at this result we have used $\nabla \times (-\nabla \times \boldsymbol{\Omega'}) = \Delta \boldsymbol{\Omega'} - \nabla (\nabla \cdot \boldsymbol{\Omega'})$ and $\nabla \cdot \boldsymbol{\Omega'} = 0$. The latter property is realized for the target vorticity derived from Eq. (6). For vanishing forcing, i.e. $\Omega_3^{ref} \to 0$ it becomes evident that the relaxation source term formally agrees with the viscous term of the incompressible vorticity equation with σ acting as a diffusion constant equivalent to the kinematic viscosity. From the wave-number-frequency transformation specified as

$$\hat{f}(\boldsymbol{k}, \omega) = \mathcal{F}(f(\boldsymbol{x}, t)) = \frac{1}{(2\pi)^n} \int_{-\infty}^{\infty} f(\boldsymbol{x}, t) \exp\left(i\left(\omega t - \boldsymbol{k}\boldsymbol{x}\right)\right) \mathrm{d}^n \boldsymbol{x}\mathrm{d}t, \tag{10}$$

and

$$f(\boldsymbol{x}, t) = \mathcal{F}^{-1}\left(\hat{f}(\boldsymbol{k}, \omega)\right) = \frac{1}{2\pi} \int_{-\infty}^{\infty} \hat{f}(\boldsymbol{k}, \omega) \exp\left(-i\left(\omega t - \boldsymbol{k}\boldsymbol{x}\right)\right) \mathrm{d}^n \boldsymbol{k}\mathrm{d}\omega, \tag{11}$$

where n indicates the dimension of the problem, the Fourier transform of the model vorticity equation becomes

$$-i\omega \hat{\Omega}'_3 + ik_1 v_1^0 \hat{\Omega}'_3 = -\sigma k^2 \left(\hat{\Omega}'_3 - \hat{\Omega}_3^{ref} \right) \tag{12}$$

with $k = |\boldsymbol{k}|$. For constant σ the right-hand side relaxation term agrees in form with the corresponding Fourier transform of the right-hand side of Eq. (4), albeit with the relaxation parameter σ replaced by σk^2, i.e. the coupling to the reference solution apparently becomes wave-number selective, i.e. seemingly enforces a closer matching with the reference solution with increasing wave number. However, one has to take into account that the excitation from turbulence will impose specific wave-number-frequency characteristics. To reveal this behavior, first from the previous relationship Eq. (12) the following transfer function between target and excitation function is obtained

$$\hat{\Omega}'_3 = \underbrace{\frac{\sigma k^2}{\sigma k^2 - i\left(\omega - k_1 v_1^0\right)}}_{T(k,\omega)} \hat{\Omega}_3^{ref} \tag{13}$$

American Institute of Aeronautics and Astronautics

The vorticity wave-number-frequency spectrum of excited vorticity $\Phi(\boldsymbol{k}, \omega)$ is related to a homogeneous and stationary forcing cross-spectrum via

$$\Phi\left(\boldsymbol{k}, \omega\right) = \left|T\left(\boldsymbol{k}, \omega\right)\right|^2 \Phi^{ref}\left(\boldsymbol{k}, \omega\right), \quad \left|T\left(\boldsymbol{k}, \omega\right)\right|^2 = \frac{\sigma^2 k^4}{\sigma^2 k^4 + \left(\omega - k_1 v_1^0\right)^2}, \tag{14}$$

refer to the discussion in Appendix A. The vorticity spectrum used as the reference solution in the previous equation is the wave-number-frequency Fourier transform of the vorticity two-point cross-correlation function

$$R(\boldsymbol{r}, \tau) = \langle \Omega_3'(\boldsymbol{x}, t) \Omega_3'(\boldsymbol{x} + \boldsymbol{r}, t + \tau) \rangle, \tag{15}$$

or

$$\Phi^{ref}\left(\boldsymbol{k}, \omega\right) = \mathcal{F}\left(R(\boldsymbol{r}, \tau)\right) \tag{16}$$

To gain insight into the forcing behavior, next we use a simplified vorticity two-point cross-correlation function assuming frozen turbulence of turbulent length scale l and variance $\hat{R}$,

$$R(\boldsymbol{x}, \tau) = \hat{R} \exp\left[-\frac{\ln(2)}{l^2}\left(\left(x_1 - v_1^0 \tau\right)^2 + x_2^2\right)\right]. \tag{17}$$

A correlation length much smaller than that observed for velocity would be expected for vorticity. Applying the spatio-temporal Fourier transformation to this expression yields (refer to Appendix B)

$$\Phi^{ref}\left(\boldsymbol{k}, \omega\right) = \frac{\hat{R} l^2}{2 \ln(2)} \exp\left(-\frac{k^2 l^2}{4 \ln(2)}\right) \delta\left(\omega - k_1 v_1^0\right), \tag{18}$$

where δ denotes the Dirac delta function. The frequency spectrum of the reference solution is the time Fourier transform of $R(\boldsymbol{0}, \tau)$, which infers from the previous vorticity spectrum

$$S^{ref}(\omega) = \int \Phi^{ref}\left(\boldsymbol{k}, \omega\right) \exp\left(i\boldsymbol{k}\boldsymbol{0}\right) \mathrm{d}^n \boldsymbol{k} = \int \Phi^{ref}\left(\boldsymbol{k}, \omega\right) \mathrm{d}^n \boldsymbol{k}. \tag{19}$$

Corresponding straight forward integration of Eq. (18) yields

$$S^{ref}(\omega) = \sqrt{\frac{\pi}{\ln(2)}} \frac{\hat{R} l}{|v_1^0|} \exp\left(-\frac{\omega^2 l^2}{4 \ln(2)(v_1^0)^2}\right). \tag{20}$$

Similarly, the excited spectrum is obtained by the integral

$$S(\omega) = \int \Phi\left(\boldsymbol{k}, \omega\right) \mathrm{d}^n \boldsymbol{k} = \int \left|T\left(\boldsymbol{k}, \omega\right)\right|^2 \Phi^{ref}\left(\boldsymbol{k}, \omega\right) \mathrm{d}^n \boldsymbol{k}. \tag{21}$$

The integral is derived in Appendix C. The forced spectrum becomes

$$S(\omega) = \sqrt{\frac{\pi}{\ln(2)}} \frac{\hat{R} l}{|v_1^0|} \exp\left(-\frac{\omega^2 l^2}{4 \ln(2)(v_1^0)^2}\right), \tag{22}$$

i.e. equals the forcing spectrum Eq. (19). That is, the transfer function between the reference frequency spectrum and the forced spectrum has an all-pass characteristic,

$$\left|\mathcal{T}_\omega\right|^2 = \frac{S(\omega)}{S^{ref}(\omega)} = 1. \tag{23}$$

Note, in practical numerical application a high-frequency cut-off must be expected for wave-numbers not resolved by the applied numerical mesh. Furthermore, numerical damping will cause deviations from the previous results. For example, the effect of numerical damping can be estimated in the previous model by introducing a slightly higher relaxation parameter for the resulting solution, i.e. using the right-hand side $\sigma_1 \partial^2 \Omega_3' / \partial x_i^2 - \sigma \partial^2 \Omega_3^{ref} / \partial x_i^2$, where the difference $\sigma_1 - \sigma = \nu_d$ could be deemed to represent the effect of an additional numerical viscosity. As a consequence, the transfer function changes to

$$\left|\mathcal{T}_\omega\right|^2 = \left(1 + \frac{\nu_d}{\sigma}\right)^{-2}, \tag{24}$$

i.e. causes a broadband amplitude loss. To overcome those losses, practically the actual scaling parameter must be chosen considerable higher than the numerical damping loss, i.e. $\sigma \gg \nu_d$. Finally, in the previous frozen turbulence model the turbulence convection velocity exactly complies with the numerical convection velocity. For decaying turbulence and more complex flow, where the convection prescribed by the source model and the actual convection velocity as realized by the governing equations solved differ, additional losses might be expected. The previous model problem is studied numerically in Section IV.D for frozen and decaying turbulence. Please refer to this section for further discussion. Similar to the previous discussion, a wave-number transfer function derives from integrating Eq. (14) over all frequencies,

$$\Psi^{ref}(\boldsymbol{k}) = \int \Phi^{ref}(\boldsymbol{k},\omega)\mathrm{d}\omega, \quad \Psi(\boldsymbol{k}) = \int |T(\boldsymbol{k},\omega)|^2 \, \Phi(\boldsymbol{k},\omega)\mathrm{d}\omega, \tag{25}$$

and computing

$$|\mathcal{T}_k|^2 := \frac{\Psi}{\Psi^{ref}}. \tag{26}$$

For the datum model, straight forward integration yields the wave-number transfer function

$$|\mathcal{T}_k|^2 = 1, \tag{27}$$

i.e. an all-pass characteristic for all wave-numbers.

The previous result further highlights that the third goal as specified at the beginning of the previous section, i.e. a wave-number selective forcing, cannot be obtained by the simplest relaxation model proposed above. To accomplish this feature, a wave-number artificial selective damping akin to the method proposed by Tam & Webb[13] might be necessary to replace the previous relaxation parameter σ. Furthermore, a wave-number selective forcing can be obtained using the hyperviscosity relaxation

$$\frac{\partial v_i'}{\partial t} + \cdots = \epsilon_{ijk}\frac{\partial}{\partial x_j}\left[\frac{\partial^2}{\partial x_l^2}\sigma\left(\Omega_k' - \Omega_k^{ref}\right)\right]. \tag{28}$$

By transforming the simplified 2-D uniform flow model discussed before with the relaxation term Eq. (28) into a 2-D vorticity equation, the resulting transfer function equivalent to Eq. (13) becomes

$$T(\boldsymbol{k},\omega) = \frac{\sigma k^4}{(\sigma k^4 + \nu_d k^2) - i\left(\omega - k_1 v_1^0\right)}, \tag{29}$$

Figure 2. Theoretical high-pass characteristic of a hyperviscosity relaxation source for the considered model problem.

where also the effect of a numerical and/or eddy dissipation is accounted for via an efficient numerical model viscosity ν_d. The finally resulting wave-number transfer function becomes

$$|\mathcal{T}_k|^2 = \frac{k^4}{\left(k^2 + \frac{\nu_d}{\sigma}\right)^2}, \tag{30}$$

which realizes a high-pass filter of cross-over wave-number $k_c = \sqrt{\nu_d/\sigma}$ and 12dB/octave slope. The filter characteristic is shown in Fig. 2 for a wave-number normalized with the cross-over wave-number.
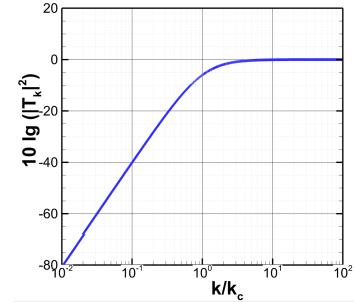
E. Sizing of relaxation parameter

In this paper we will study numerically the features of the simplest relaxation model with the LEE as presented in Eqs. (1-3). In principle, the relaxation parameter can be chosen arbitrary high, since its magnitude defines only how close source and target solution become coupled. Practically, explicit time integration usually applied for CAA could trigger numerical instabilities for a value too high of the parameter σ. As was stated already, the relaxation source Eq. (8) shares similarities with the viscous terms of the incompressible Navier-Stokes equations. This feature can help to derive meaningful magnitudes for the relaxation parameter. For large eddy simulation (LES) Dantinne et al.[14] have successfully applied viscosity and hyperviscosity models of the form given by the rhs of Eqs. (8) and (28) with $\Omega_k^{ref} \equiv 0$ and σ replaced by an eddy viscosity ν_{SGS} derived from a Smagorinsky model. An eddy viscosity derived from RANS modeling

American Institute of Aeronautics and Astronautics

usually is high enough to enforce a steady state solution. Hence, a value $\sigma = \nu_t$ derived from RANS eddy viscosity might be a meaningful estimate to accomplish with the relaxation source term a close coupling between target and reference solution.

The eddy relaxation source with high value of σ applied in a forcing zone embedded in the computational domain in conjunction with fluctuating vorticity determined from RANS turbulence statistics can be used to generate inflow turbulence for scale resolving simulation downstream of the forcing zone. Note, the forcing zone is transparent for acoustic waves. If the Navier-Stokes equations in appropriate perturbation form are solved, gradually lowering the relaxation parameter in an area downstream of the forcing zone to a value $\sigma = \nu_{SGS}$ derived from a sugrid-stress model and switching off the forcing formally provides a transition from a RANS enforced turbulence to an LES model based on the Dantinne et al.[14] subgrid-stress model. However, the forcing has not necessarily to be spatially limited to the inflow forcing domain. The relaxation term in combination with the reference solution e.g. prescribed by stochastic source modeling, applied also in the LES zone will provide exactly the same subgrid model for wave-numbers higher than the cut-off wave-number k_{max} realized by the forcing model (for $k > k_{max}$ the forcing goes to zero, i.e. $\hat{\Omega}_3^{ref}(k, \omega) \to 0$). Below this cut-off, the relaxation term will fill-up the drain otherwise realized by unforced subgrid-scale model over all resolved wave-numbers and supports back scattering of the energy to the resolved scales. Hence, a variation of the relaxation parameter may provide a way to smoothly switch between zones with fully deterministic noise source modeling and zones where weakly forced scale resolving simulation is applied.

III.   Non-linear perturbation equations

To proceed forward to the use of general non-linear governing equations the DLR CAA code PIANO[15] has been augmented with viscous terms. For this, the governing Navier-Stokes equations have been reformulated in perturbation form based on primitive variables. The reformulated governing equations are sketched in the subsequent section. First results of a direct noise simulation of a laminar cylinder in a cross flow are presented in Section IV.B, reflecting their proper implementation.

A.   Reformulation of the Navier-Stokes equations in perturbation form

The Navier-Stokes equations in primitive notation for compressible flow and an ideal Gas are given with $\alpha_1 = 0$ by

$$\frac{\partial \rho}{\partial t} + v_i \frac{\partial \rho}{\partial x_i} + \rho \frac{\partial v_i}{\partial x_i} = 0 \tag{31}$$

$$\frac{\partial v_i}{\partial t} + v_j \frac{\partial v_i}{\partial x_j} + \frac{1}{\rho} \frac{\partial p}{\partial x_i} - \frac{1}{\rho} \frac{\partial \tau_{ij}}{\partial x_j} = -\alpha_1 \left[\frac{1}{\rho} \frac{\partial (\tau_{ij})_{sgs}}{\partial x_j} \right] \tag{32}$$

$$\frac{\partial p}{\partial t} + v_i \frac{\partial p}{\partial x_i} + \gamma p \frac{\partial v_i}{\partial x_i} - (\gamma - 1) \left[\tau_{ij} \frac{\partial v_i}{\partial x_j} - \frac{\partial q_i}{\partial x_i} \right] = \alpha_1 \, \vartheta_{sgs}. \tag{33}$$

Here, the summation convention is applied and τ_{ij} and q_i indicates the viscous stress tensor and the heat flux vector. For $\alpha_1 = 1$ the equation system corresponds to the spatially filtered Navier-Stokes equations in primitive variables usable for Large Eddy Simulation (LES). It includes additional subgrid scale (SGS) stress[a] and heat flux contributions $(\tau_{ij})_{sgs}$ and ϑ_{sgs} on the right-hand side. Note, for $\alpha_1 = 1$ the flow variables implicitly represent spatially Favre filtered quantities (the spatial filtering indicated by $\langle \cdots \rangle$). Let ρ^*, v_i^*, and p^* denote the unfiltered velocity in case $\alpha_1 = 1$. Then, the flow variables for $\alpha_1 = 1$ represent $\rho = \langle \rho^* \rangle$, $v_i = \langle \rho^* v_i^* \rangle / \langle \rho^* \rangle$, and $p = \langle p^* \rangle$. Furthermore, the subgrid stresses are defined by $(\tau_{ij})_{sgs} = \langle \rho^* \rangle \left(\langle v_i^* v_j^* \rangle - \langle v_i^* \rangle \langle v_j^* \rangle \right)$ and can be obtained from functional modeling. In general, the subgrid terms are defined as a function of the Favre filtered flow variables; their actual formulation depends on the explicit SGS-model applied.

To accomplish a formulation of the Navier-Stokes equations in non-linear perturbations of primitive variables, the dependent variables are split into base flow parts ρ^0, v_i^0, p^0, and fluctuations indicated by a prime,

$$\rho = \rho^0 + \rho', \quad v_i = v_i^0 + v_i', \quad p = p^0 + p', \quad \tau_{ij} = \tau_{ij}^0 + \tau_{ij}', \quad q_i = q_i^0 + q_i'. \tag{34}$$

---

[a]The sign of this term corresponds to the definition as usual used for LES modeling.

The primitive base flow variables in general represents a steady or unsteady given flow (we use the notion base-flow rather than mean-flow here to underline that the flow could be unsteady). Note, the fluctuating stress tensor τ'_{ij} and τ^0_{ij} denote viscous contributions, i.e. they do not designate turbulent Reynolds stress components (turbulent stresses of the base flow will be designated in the following by $\left(\tau^0_{ij}\right)_{turb}$ and mean turbulent heat fluxes via $\left(q^0_i\right)_{turb}$). Replacing all variables in the Navier-Stokes equations by the previous decomposition and rearrangement using the definition of the complete mean and fluctuating stress tensors $\sigma^0_{ij} := \tau^0_{ij} - p^0 \delta_{ij}$, respectively $\sigma'_{ij} := \tau'_{ij} - p' \delta_{ij}$, yields

$$\frac{\partial \rho'}{\partial t} + \frac{\partial}{\partial x_i}\left(\rho' v_i + \rho^0 v'_i\right) = m^0 \tag{35}$$

$$\frac{\partial v'_i}{\partial t} + v_j \frac{\partial v'_i}{\partial x_j} + v'_j \frac{\partial v^0_i}{\partial x_j} - \frac{1}{\rho}\frac{\partial \sigma'_{ij}}{\partial x_j} + \frac{\rho'}{\rho \rho^0}\frac{\partial \sigma^0_{ij}}{\partial x_j} = f^0_i \tag{36}$$

$$\frac{\partial p'}{\partial t} + \frac{\partial}{\partial x_i}\left(p' v_i + p^0 v'_i\right) - (\gamma - 1)\left(\sigma'_{ij}\frac{\partial v_i}{\partial x_j} + \sigma^0_{ij}\frac{\partial v'_i}{\partial x_j} - \frac{\partial q'_j}{\partial x_j}\right) = \vartheta^0, \tag{37}$$

with the residual right-hand source terms given by

$$m^0 = -\left[\frac{\partial \rho^0}{\partial t} + \frac{\partial}{\partial x_j}\left(\rho^0 v^0_j\right)\right] \tag{38}$$

$$f^0_i = -\left[\frac{\partial v^0_i}{\partial t} + v^0_j \frac{\partial v^0_i}{\partial x_j} + \frac{1}{\rho^0}\frac{\partial p^0}{\partial x_i} - \frac{1}{\rho^0}\frac{\partial \tau^0_{ij}}{\partial x_j}\right] - \alpha_1 \left[\frac{1}{\rho}\frac{\partial (\tau_{ij})_{sgs}}{\partial x_j}\right] \tag{39}$$

$$\vartheta^0 = -\left[\frac{\partial p^0}{\partial t} + v^0_i \frac{\partial p^0}{\partial x_i} + \gamma p^0 \frac{\partial v^0_i}{\partial x_i} - (\gamma - 1)\left(\tau^0_{ij}\frac{\partial v^0_i}{\partial x_j} - \frac{\partial q^0_i}{\partial x_i}\right)\right] + \alpha_1\, \vartheta_{sgs}. \tag{40}$$

Note, the quantities that do not have a prime or a superscript are total quantities, and when combined with primed quantities produce nonlinear terms. In general, any base flows is supposed to satisfy

$$\frac{\partial \rho^0}{\partial t} + \frac{\partial}{\partial x_j}\left(\rho^0 v^0_j\right) = 0 \tag{41}$$

$$\frac{\partial v^0_i}{\partial t} + v^0_j \frac{\partial v^0_i}{\partial x_j} + \frac{1}{\rho^0}\frac{\partial p^0}{\partial x_i} - \frac{1}{\rho^0}\frac{\partial \tau^0_{ij}}{\partial x_j} = \alpha_2 \left[\frac{1}{\rho^0}\frac{\partial \left(\tau^0_{ij}\right)_{turb}}{\partial x_j}\right] \tag{42}$$

$$\frac{\partial p^0}{\partial t} + v^0_i \frac{\partial p^0}{\partial x_i} + \gamma p^0 \frac{\partial v^0_i}{\partial x_i} - (\gamma - 1)\left(\tau^0_{ij}\frac{\partial v^0_i}{\partial x_j} - \frac{\partial q^0_i}{\partial x_i}\right) = \alpha_2\,(\gamma - 1)\left[\left(\tau^0_{ij}\right)_{turb}\frac{\partial v^0_i}{\partial x_j} - \frac{\partial (q_i)_{turb}}{\partial x_i}\right]. \tag{43}$$

From this the residual right-hand side sources of the perturbation equation system Eqs. (35-37) infer as

$$m^0 \quad = \quad 0 \tag{44}$$

$$f^0_i \quad = \quad -\alpha_2 \left[\frac{1}{\rho^0}\frac{\partial \left(\tau^0_{ij}\right)_{turb}}{\partial x_j}\right] - \alpha_1 \left[\frac{1}{\rho}\frac{\partial (\tau_{ij})_{sgs}}{\partial x_j}\right] \tag{45}$$

$$\vartheta^0 \quad = \quad -\alpha_2\,(\gamma - 1)\left[\left(\tau^0_{ij}\right)_{turb}\frac{\partial v^0_i}{\partial x_j} - \frac{\partial (q_i)_{turb}}{\partial x_i}\right] + \alpha_1\, \vartheta_{sgs}. \tag{46}$$

For $\alpha_2 = 0$ the base-flow system (41-43) corresponds to Eqs. (35-37) with $\alpha_1 = 0$, i.e. the base flow represents an unsteady solution to the Navier-Stokes equations. In this case ($\alpha_1 = 0$ and $\alpha_2 = 0$) all residual right-hand side sources in Eqs. (44-46) are identical zero. Then, the fluctuations ρ', v'_i, and p' describe small perturbations on top of the (unsteady) Navier-Stokes base flow given by ρ^0, v^0_i, and p^0, where the total solution of base-flow and fluctuations superposed also satisfies the Navier-Stokes equations. This formulation, for example, allows to study the scattering of acoustic waves (included in the fluctuations) in a prescribed turbulent flow field (given by the base-flow).

For $\alpha_2 = 1$ and $\alpha_1 = 0$ the base flow represents a steady compressible RANS solution, if the right-hand side terms of Eqs. (41-43) are determined by the RANS modeled Reynolds stresses and turbulent heat fluxes, i.e.

$$\left(\tau^0_{ij}\right)_{turb} = -\overline{\rho v''_i v''_j}, \tag{47}$$

and

$$(q_i)_{turb} = -c_p \overline{\rho v_i'' T''}. \tag{48}$$

Since $\alpha_2 = 1$ these terms will provide constant contributions to the residual terms in Eqs. (44-46). The base flow variables represent Favre averaged flow quantities. That is, $v_i^0 := \widetilde{v}_i$, $\rho^0 := \bar{\rho}$, and $p^0 := \bar{p}$. Hence, $v_i' = v_i - v_i^0 = v_i - \widetilde{v}_i = v_i''$. The major effect of the resulting steady residual terms on the right-hand side of the system Eqs. (35-37) is to balance non-vanishing mean contributions that come from the non-linear terms on the left-hand side to accomplish fluctuations with zero Favre average.

The perturbation formulation of the Navier-Stokes equations over a steady RANS mean flow is given by $\alpha_1 = 0$ and $\alpha_2 = 1$. It would be suitable for Direct Numerical Simulation (DNS) of turbulent flow, where the fluctuations represent the unsteady part of the DNS simulation (a sufficient fine mesh resolution provided). Since the governing perturbation equations include acoustic contributions, also Direct Noise Computation (DNC) of turbulent sound generation and propagation would be possible on sufficiently extended meshes. Possible differences in the exact (i.e. DNS averaged) mean flow and the approximative RANS base-flow show up in the solution as a non-vanishing mean contribution from the resolved fluctuations, e.g. $\overline{\rho v_i'} \simeq \overline{v_i'} = 0$. DNC results for a laminar vortex shedding cylinder are presented in Section IV.B to further highlight application of this approach (refer also to Figures 5 and 6).

For an overset Large-Eddy Simulation,[16] the fluctuations represent the unsteady resolved part of the LES simulation over a RANS base flow, i.e. $v_i' := \langle \rho^* v_i^* \rangle / \langle \rho^* \rangle - \widetilde{v}_i$, $v_i^0 := \widetilde{v}_i$. This implies that the right-hand side residual terms include besides the steady contributions additional unsteady contributions specified by the subgrid scale (SGS) model applied (i.e. $\alpha_1 = 1$, $\alpha_2 = 1$). Theses additional right-hand side terms plus the steady residual terms from the RANS mean-flow constitute the unsteady right-hand side residual terms

$$m^0 \;=\; 0 \tag{49}$$

$$f_i^0 \;=\; -\left[\frac{1}{\rho^0}\frac{\partial\left(\tau_{ij}^0\right)_{turb}}{\partial x_j}\right] - \left[\frac{1}{\rho}\frac{\partial(\tau_{ij})_{sgs}}{\partial x_j}\right] \tag{50}$$

$$\vartheta^0 \;=\; -(\gamma-1)\left[\left(\tau_{ij}^0\right)_{turb}\frac{\partial v_i^0}{\partial x_j} - \frac{\partial(q_i)_{turb}}{\partial x_i}\right] + \vartheta_{sgs}. \tag{51}$$

Compared to the LEE, the perturbation system Eqs. (35-37) over a RANS mean-flow ($\alpha_2 = 1$) demands for additional storage of the (symmetric) mean-flow stress tensor τ_{ij}^0 (or σ_{ij}^0), its divergence $\partial\tau_{ij}^0/\partial x_j$, the constant contribution to the residual right-hand side source f_i^0, i.e. $\partial\left(\tau_{ij}^0\right)_{turb}/\partial x_j$, and the constant contribution to ϑ^0 (specified by Eq. (46)). This in total yields 13 quantities for each mesh point.

In case of a base flow taken from steady RANS ($\alpha_2 = 1$), all time-derivative terms are equal zero, e.g. $\partial v_i^0/\partial t = 0$ in Eq. (42) and the amount of mean-flow data stored permanently can be reduced further. The momentum equation Eq. (42) can be used to substitute the last left-hand side term of Eq. (36) by

$$\frac{\rho'}{\rho\rho^0}\frac{\partial\sigma_{ij}^0}{\partial x_j} = -\frac{\rho'}{\rho\rho^0}\frac{\partial\left(\tau_{ij}^0\right)_{turb}}{\partial x_j} + \frac{\rho'}{\rho}v_j^0\frac{\partial v_i^0}{\partial x_j}.$$

This yields

$$\frac{\partial\rho'}{\partial t} + \frac{\partial}{\partial x_i}\left(\rho' v_i + \rho^0 v_i'\right) = 0 \tag{52}$$

$$\frac{\partial v_i'}{\partial t} + v_j\frac{\partial v_i'}{\partial x_j} + v_j'\frac{\partial v_i^0}{\partial x_j} + \frac{\rho'}{\rho}v_j^0\frac{\partial v_i^0}{\partial x_j} - \frac{1}{\rho}\frac{\partial\sigma_{ij}'}{\partial x_j} = \hat{f}_i^0 \tag{53}$$

$$\frac{\partial p'}{\partial t} + \frac{\partial}{\partial x_i}\left(p' v_i + p^0 v_i'\right) - (\gamma-1)\left(\sigma_{ij}'\frac{\partial v_i}{\partial x_j} + \sigma_{ij}^0\frac{\partial v_i'}{\partial x_j} - \frac{\partial q_j'}{\partial x_j}\right) = \vartheta^0, \tag{54}$$

with

$$\hat{f}_i^0 = -\left[\frac{1}{\rho}\frac{\partial\left(\tau_{ij}^0\right)_{turb}}{\partial x_j}\right] - \left[\frac{1}{\rho}\frac{\partial(\tau_{ij})_{sgs}}{\partial x_j}\right]\alpha_1 \tag{55}$$

The number of additional mean-flow variables to be permanently stored reduces to 10, i.e. 6 for the viscous mean-stress tensor σ_{ij}^0 (or τ_{ij}^0), 3 for $\partial\left(\tau_{ij}^0\right)_{turb}/\partial x_j$ in $\hat{f}_i$, and 1 for ϑ^0. The system given by Eqs. (52-54) is the main result of this section and has been implemented into the DLR CAA code PIANO.[15]

The non-linear perturbation equations given by Eqs. (52-54) reduce to the PENNE equations proposed by Long[17] if all viscous terms are neglected. Non-linear disturbance equations (NLDE) starting from a conservative form of the Navier-Stokes equations have been proposed by Morris et al. and Liu & Long.[18, 19] Large Eddy Simulations based on the NLDE have been reported by Terracol.[20, 21]

Subsequently, we will refer to the previously derived non-linear perturbation equations given by Eqs. (35-37) and Eqs. (52-54) (and a simplification of it discussed in the next section) as NLPE.

B. Subsonic approximation

Tam and Kurbatski[22–24] have used Eq. (36) in a slightly modified form for a direct numerical simulation (DNS) of flow induced sound generation in flow problems of moderate Mach number of order $M_\infty = 0.1$. In their simulations the right-hand side terms of the pressure equation are omitted. Furthermore, the viscous right-hand side term of the momentum equation is computed based on a constant viscosity ($\mu = const.$). Their modified equation system reads

$$\frac{\partial \rho}{\partial t} + v_i \frac{\partial \rho}{\partial x_i} + \rho \frac{\partial v_i}{\partial x_i} = 0$$

$$\frac{\partial v_i}{\partial t} + v_j \frac{\partial v_i}{\partial x_j} + \frac{1}{\rho}\frac{\partial p}{\partial x_i} - \frac{1}{\rho}\frac{\partial \tau_{ij}}{\partial x_j} = -\left[\frac{1}{\rho}\frac{\partial (\tau_{ij})_{sgs}}{\partial x_j}\right]\alpha_1 \tag{56}$$

$$\frac{\partial p}{\partial t} + v_i \frac{\partial p}{\partial x_i} + \gamma p \frac{\partial v_i}{\partial x_i} = 0,$$

with $\alpha_1 = 0$ (for $\alpha_1 = 1$ it represents their spatially filtered version with subgrid stress contributions included). The modification essentially means to neglect any temperature effects in the combined flow and aeroacoustic simulation. The drop of the viscous dissipation term means to neglect the temperature effect onto the solution due to the transformation of mechanical into thermal energy. Note, the removal of mechanical energy is still accomplished by the right-hand side source term of the momentum equation.

In an incompressible simulation of turbulence the temperature field is decoupled from the flow simulation. Since an incompressible solution is known to represent a good approximative to flow of small to moderate Mach number, the simplification is reasonable for the flow solution in this regime.

Acoustically, the right-hand side terms of the pressure equation represent heat sources due to the viscous dissipation of mechanical energy. For small Mach numbers their contribution is negligible.

Physical good results based on this formulation of the Navier-Stokes equations have been reported by Tam et al. for the direct numerical simulation of the attenuation of acoustic waves at liners[22, 23] and the laminar tone generation at the trailing edge of a NACA0012 airfoil.[24] A perturbation version of the Navier-Stokes equations in the form of Eqs. (52-54) reads

$$\frac{\partial \rho'}{\partial t} + \frac{\partial}{\partial x_i}\left(\rho' v_i + \rho^0 v_i'\right) = 0 \tag{57}$$

$$\frac{\partial v_i'}{\partial t} + v_j \frac{\partial v_i'}{\partial x_j} + v_j' \frac{\partial v_i^0}{\partial x_j} + \frac{\rho'}{\rho}v_j^0 \frac{\partial v_i^0}{\partial x_j} - \frac{1}{\rho}\frac{\partial \sigma_{ij}'}{\partial x_j} = \hat{f}_i^0 \tag{58}$$

$$\frac{\partial p'}{\partial t} + v_i \frac{\partial p'}{\partial x_i} + v_i' \frac{\partial p^0}{\partial x_i} + \gamma p^0 \frac{\partial v_i'}{\partial x_i} + \gamma p' \frac{\partial v_i}{\partial x_i} = \vartheta^0. \tag{59}$$

In this case the right-hand side residual term $\hat{f}_i^0$ is given by Eq. (55), while ϑ^0 equals

$$\vartheta^0 = -\left[\frac{\partial p^0}{\partial t} + v_i^0 \frac{\partial p^0}{\partial x_i} + \gamma p^0 \frac{\partial v_i^0}{\partial x_i}\right]. \tag{60}$$

The base flow is derived from a steady RANS solution ($\alpha_2 = 1$), hence, the residual term becomes

$$\vartheta^0 = -(\gamma - 1)\left(\left(\tau_{ij}^0\right)_{turb}^+ \frac{\partial v_i^0}{\partial x_j} - \frac{\partial (q_i)_{turb}^+}{\partial x_i}\right), \tag{61}$$

where $\left(\tau_{ij}\right)_{turb}^+ = \left(\tau_{ij}^0\right)_{turb} + \tau_{ij}^0$ denotes the total stress tensor from RANS, including viscous and turbulent contributions, and $(q_i)_{turb}^+ = (q_i)_{turb} + q_i$ the corresponding total heat flux vector based on the turbulent

and viscous contributions. In case of a RANS mean-flow, the number of additional mean-flow variables to be permanently stored reduces to 4, i.e. 3 for $\partial\left(\tau_{ij}^0\right)_{turb}/\partial x_j$ in $\hat{f}_i$, and 1 for ϑ^0.

Compared to the linearized Euler equations, besides the constant right-hand side sources (and possible contributions of subgrid scale stresses for $\alpha_1 = 1$), the equations differ only in the additional shear stress terms in $\partial\sigma_{ij}/\partial x_j = \partial\tau_{ij}/\partial x_j - \delta_{ij}\partial p/\partial x_j$.

IV.   Numerical results

A.   CAA code

CAA computations have been carried out with the DLR Code PIANO.[15] PIANO is a structured multi-block method using curvilinear meshes. The code is parallelized and the spatial discretization is based on the DRP scheme proposed by Tam and Webb.[13] Metric coefficient are also computed with the DRP scheme. To remove spurious waves, artificial selective damping[13] and different filters are available. Explicit time integration is applied using a standard A-stable Runge Kutta method that supports fourth order accuracy also for non-linear perturbation equations. At the far-field boundaries radiation and outflow boundary conditions of Tam and Webb are applied that can be augmented by a sponge zone if additional damping e.g. of vorticity waves at an outflow boundary is needed. For the inviscid equations a kinematic adiabatic wall boundary condition is implemented that uses one layer of ghost point exterior to the surface of the body fitted mesh. The ghost values are predefined for each simulation step such as to properly enforce the boundary condition. For the viscous equations the ghost point concept has been successfully extended to a no-slip boundary condition by prescribing those three components of the complete fluctuating shear stress tensor σ'_{ij} on the ghost points, which affect the wall normal derivative of the divergence of the shear-stress tensor in the momentum equation. The code solves non-dimensionalized equations, using as reference quantities density ρ_{ref}, speed of sound c_{ref}, and a reference length l_{ref}. For viscous simulations, this information is augmented by a Mach and Reynolds number related to the problem. The stochastic forcing is realized with the Fast Random Particle-Mesh method.[6–8] Fluctuating vorticity is passed during each full Runge-Kutta cycle to the CAA code. Intermediate source term levels are computed by appropriate interpolation between four stored consecutive source time levels. The curl of difference of fluctuating vorticity and fluctuating vorticity from FRPM is computed by an additional application of the DRP scheme.

B.   Laminar cylinder in a cross flow

1.   Computational set up

To test the proper NLPE implementation in PIANO, a Direct Noise Computation (DNC) of a laminar vortex shedding cylinder problem was simulated for three different Mach numbers, i.e. M=0.1, 0.2 and 0.3. The Reynolds number corresponds to Re=150. The test case corresponds to the one published by Inoue & Hatakeyama.[25] For spatial discretization the fourth-order accurate DRP scheme of Tam & Webb[13] is used. The fourth-order standard Runge-Kutta scheme is used for time integration. The CAA grid consists of 16 blocks and is shown in Figure 3(a). The total number of grid points are 400.964, where 168 grid points are distributed on the cylinder surface. The grid topology close to the cylinder surface is shown in Figure 3(b).

Adiabatic and no-slip wall conditions are adopted on the cylinder surface and radiation boundary conditions (Tam & Webb 1993) are used at the outer boundary of the computational domain. Additionally, a sponge layer is prescribed at the outflow boundaries such that acoustic on a continuous waves damp out in the sponge zone and become sufficiently small before reaching the outer boundary of the computational domain, where additionally radiation boundary conditions are employed. As for such a laminar flow, the thickness of the boundary layer is estimated by $\delta \sim 1/\sqrt{\mathrm{Re}}$ and it is calculated $\delta \sim 0.08$ for Re = 150 (in CFD). For the CAA grid, the initial grid spacing to the wall is chosen as $\delta = 0.05$. In order to resolve acoustic waves the lowest acoustic resolution should be 10 points per wave length (PPW) which is more than two times the theoretical resolution limit 5.4 PPW for DRP scheme. In the wake of the cylinder the resolution requirement is defined by the size of the vortex street. The characteristic wave-length in the wake behind the cylinder is $\lambda/D = St^{-1} \approx 5.46D$. Hence, with 10 PPW, a spacing of $\Delta x = 0.5D$ is needed. In this work for all computations the spacing is fixed to $\Delta x = 0.2D$. This grid spacing is based on many preliminary tests were done by Inoue et al.[25] The mean flow solutions are non-dimensionalized. Especially, the non-dimensional time scale is derived from $T_{ref} = D/c_\infty$. CFD results are interpolated onto the CAA
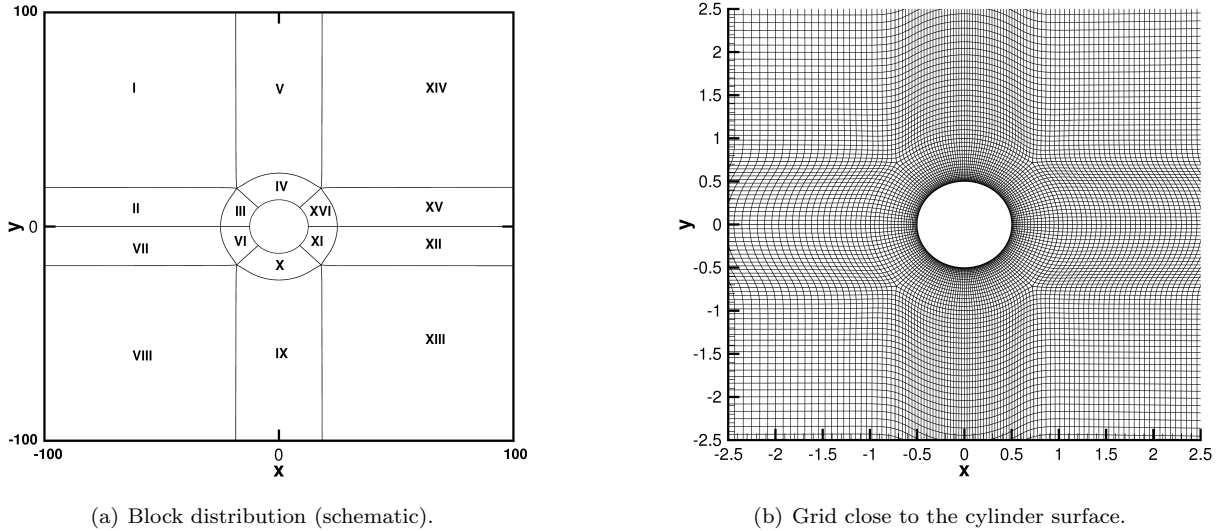
(a) Block distribution (schematic).

(b) Grid close to the cylinder surface.

Figure 3. CAA topology and grid used for the cylinder test case.

mesh. After some preliminary simulations, the depth of the sponge layer is chosen to be $30D$. The time step is chosen $\Delta t = 1.5 \times 10^{-3}$, based on an inviscid $(\Delta t)_{\text{CFL}} = 5.4 \times 10^{-3}$ and the grid on the cylinder surface.

2. Computational results

Good agreement of PIANO results with results from literature could be observed.[25] The base flow of the unsteady simulations is taken from a RANS simulation of the half cylinder problem, thus suppressing the onset of vortex shedding in the RANS simulation by enforcing symmetry, Figure 4. However, this base flow in general does not agree with the actual time averaged flow simulation of the problem including vortex shedding. Therefore, the fluctuations provided by the CAA simulation have a non-vanishing mean that provides a correction to the initial mean-flow field from RANS. Figure 5-6 present the RANS mean-flow, the mean-flow with corrections from CAA (PIANO), pure fluctuations from CAA and the total flow field of the combined base flow with fluctuations from CAA. Snapshots of unsteady vorticity are shown in Figure 7-9. The vorticity length scale show similar scales for different Mach numbers $M = 0.1$, $M = 0.2$, and $M = 0.3$. Finally, contour plots of radiated pressure are shown in Figure 10-12. It is evident that with increasing Mach number the acoustic wave-length of the radiated waves decreases. The simulations reveal a proper implementation of the additional viscous terms.

C. Relaxation model test case 1: unstable jet

To test the capabilities of the relaxation source term Eq. (8) to properly control vorticity levels while leaving acoustic wave propagation unharmed, the category 4 problem 1 test case of the 4th CAA Workshop on Benchmark Problems has been selected.[9] The problem consists of an energy source inside a two-dimensional jet that generates an acoustic wave that is refracted as it moves through the jet shear layer. The problem solved with the linearized Euler equations posses a hydrodynamic instability. The benchmark problem requires the solution of the fluctuations associated only with the sound radiation and refraction through the jet, while the instability waves associated to unstable vorticity modes should be avoided.

The jet has a center line Mach number of $M_j = 0.756$ and a core temperature of $T_j = 600K$. Outside the jet the medium is at rest with temperature $T_\infty = 300K$. The mean velocity, temperature and density profile is specified analytically. The vertical velocity profile is prescribed by a Gaussian with half-width $b = 1.3m$. A lenticular shaped harmonic energy source is located on the jet axis and radiates at frequency $\omega_0 = 76 rad/s$. Further details of the definition of the test problem can be found in the 4th CAA workshop report.[9]

The simulations are carried out on a CAA mesh that extends from $x = -50$ to 150 and from $y = 0$ to 60 using a reference length $l_{ref} = 1$m. The mesh is slightly clustered so that about 20 vertical mesh points are located inside the jet. The jet center line is located at $y = 0$. Exploiting symmetries, only one

half plane is simulated in the basic set-up using a kinematic boundary condition on the jet axis. Fig. 13 presents the fluctuating pressure field at the beginning of the 8th cycle using the linearized Euler equations without relaxation source term, i.e. $\sigma = 0$. The location of the sound source at $x = 0$ is visible. Sound waves are radiated from the source. Refraction of the sound waves can be observed shaping a cone of silence downstream of the source. Furthermore, downstream of the sound source a convective instability wave with linearly growing amplitude is present in the solution.

Fig. 14 presents a solution with the relaxation source term Eq. (8) applied over the entire length of the computational domain with a vertical scaling as defined by

$$\sigma = \hat{\sigma} \exp\left(-\frac{y^2}{d^2}\right) \tag{62}$$

where $d = 2.5$ and a peak relaxation parameter $\hat{\sigma} = 0.03$ was chosen. The extension of the region where the relaxation source term is applied is indicated by the colored box in Fig. 14. No additional forcing is applied, i.e. $\Omega_3^{ref} \equiv 0$, hence the relaxation source term primarily damps out all vorticity fluctuations. Two features are evident. First, the hydrodynamic instability has been removed from the simulation. Second, the acoustic fields reveals similar acoustic sound patterns as present in the unstable solution. In particular, a cone of silence is present and sound fluctuations show the same magnitude. A further comparison for this test case can be found in Fig. 15, where different test set-ups are studied. The main parameters are listed in Table 1[b]. All cases have been run with the same time step as applied in the unstable simulation, i.e. the magnitude of the relaxation parameter does not affect numerical stability. Further details are revealed in

Table 1. **Main relaxation term parameters of different jet simulations**

case	$\hat{\sigma}$	d, Eq. (62)	x-range	y-range	x-range CAA	y-range CAA	comment
1	0.01	2.5	$-50 \ldots 150$	$0 \ldots 5$	$-50 \ldots 150$	$0 \ldots 60$	unstable
2	0.02	2.5	$-50 \ldots 150$	$0 \ldots 5$	$-50 \ldots 150$	$0 \ldots 60$	unstable
3	0.03	2.5	$-50 \ldots 150$	$0 \ldots 5$	$-50 \ldots 150$	$0 \ldots 60$	stable
4	0.05	∞	$-50 \ldots 150$	$0 \ldots 5$	$-50 \ldots 150$	$0 \ldots 60$	stable
5	0.05	∞	$-50 \ldots 150$	$0 \ldots 60$	$-50 \ldots 150$	$0 \ldots 60$	stable
6	0.05	2.5	$-50 \ldots 150$	$0 \ldots 5$	$-50 \ldots 150$	$0 \ldots 60$	stable
7	0.10	2.5	$-50 \ldots 150$	$0 \ldots 5$	$-50 \ldots 150$	$0 \ldots 60$	stable
8	0.05	2.5	$-50 \ldots 50$	$0 \ldots 5$	$-50 \ldots 150$	$0 \ldots 120$	stable
9	0.05	2.5	$-50 \ldots 150$	$-5 \ldots 5$	$-50 \ldots 150$	$-60 \ldots 60$	stable

Fig. 17 by reducing the contour levels. In the stabilized simulations a slightly different decay pattern can be observed in the cone of silence compared to the unstable reference solution. To exclude the possibility that this effect is caused by reflections from the boundaries, the simulation has been re-computed for an extended CAA domain, refer to cases 8 and 9 in Tab. 1 and to Fig. 16. These simulations reveal a similar altered asymptotic decay behavior in the cone of silence. Fig. 18 presents a comparison of fluctuating pressure with the analytical benchmark solution along two horizontal lines at $y = 15$ and $y = 50$, respectively. A fairly good collapse of most of the stable simulations with the reference simulation can be observed (the oscillation present for case 1 at $y = 15$ is caused by the intersection with the instability wave present in this case). For $y = 50$ the small differences in the cone of silence is observable as a small deviation from the reference solution for axial coordinates $x > 100$. Altogether the test case reveals that the relaxation source can control significantly vorticity levels while leaving the acoustic content almost unchanged. Although not an mathematical rigor solution to the category 4 problem 1 case is obtained, it is fair to conclude that for technical purposes a well working method is at hand to suppress the onset of hydrodynamic instabilities.

D. Relaxation model test case 2: forced turbulence in uniform 2-D flow

The second relaxation source test case involves turbulent forcing using a fluctuating source provided by FRPM.[6–8] The problem used in Section II.D is reproduced. A constant mean-flow in x-direction with

---

[b]A parameter $d = \infty$ indicates a spatially constant relaxation parameter

$M = 0.5$ is applied with the LEE as governing equations. The computational domain has an extension $-1 \ldots 1$ in both, x- and y-direction. The grid is Cartesian with spacing $\Delta x = \Delta y = 0.01$. A non-dimensional time step $\Delta t = 4.5e - 3$ is applied. The stochastic sound sources are generated on a FRPM patch of same size and resolution. The realized vorticity variance is set to $\hat{R} = 0.005$ and ramped with a squared sine function at the beginning and end of the source patch. Different relaxation parameter values are applied. The standard length scale of the realized reference vorticity was set to $l = 0.02$. In a first simulation frozen turbulence is considered, i.e. the vorticity correlation function realized by FRPM reads

$$R(\boldsymbol{x}, \tau) = \hat{R} \exp\left[-\frac{\pi}{4l^2}\left(\left(x_1 - v_1^0\tau\right)^2 + x_2^2\right)\right]. \tag{63}$$

In addition, decaying turbulence is also generated with FRPM according to the model

$$R(\boldsymbol{x}, \tau) = \hat{R} \exp\left[-\frac{\pi}{4l^2}\left(\left(x_1 - v_1^0\tau\right)^2 + x_2^2\right)\right] \exp\left(-\frac{|\tau|}{\tau_s}\right). \tag{64}$$

The characteristic decay time was chosen in all considered cases as $v_1^0\tau_s/l = 4.0$, i.e. it changes with the value of l chosen. Fig. 19(a) shows a snapshot of the FRPM reference solution. Fig. 19(b) provides for the same time instant the corresponding CAA solution. The ramping of the source can be observed as well as the decay towards the downstream boundary. Frequency spectra are evaluated for a sampling location at $x = 0$ and $y = 0$. Fig. 20(a) shows a comparison of forced and excited spectra for frozen turbulence. A quite close agreement over a wide range of frequencies is visible. The decay of the reference solution towards higher wave-numbers is caused by the realized length scale that defines via the convection velocity the frequency roll-off. The frequency transfer function Eq. (24) is computed by subtracting the excited and the forcing levels. The result is shown in Fig. 21(a] for frozen turbulence. Up to the mesh cut-off an all-pass characteristic is observable. This corresponds to the behavior as predicted from the toy model. The cut-off seen in the simulation is not affected by a length scale variation and extends even beyond the CAA mesh resolution at $f \approx 10.0$. Towards smaller wave-numbers a slight drop-off is obtained. It might be caused by the finite extension used for the computational problem. Fig. 20(b) presents the numerical frequency transfer function. The variation of length scale slightly shifts the high-frequency cut-off to smaller values. However, the cut-off always occurs for all values still beyond the meaningful CAA mesh resolution.

Similar results for decaying turbulence are presented in Figs. 20(b) and 22. From Fig. 22 it is evident that the capability of the target solution to follow the reference slightly deteriorates. However, also for this case an all-pass behavior up to the mesh cut-off is observed. The frequency transfer functions shown in Fig. 22 reveal a closer matching with increased relaxation parameter. The drop-off towards lower frequencies is slightly increased.

E. Relaxation model test case 3: high-lift noise

First preliminary results of the capability of forced eddy simulation to properly predict the sound generated at a high-lift system from CAA simulation are presented next. The simulated geometry is the F15LS model of DLR, which realizes a swept wing with sweep angle of $\beta = 30°$. The reference flow velocity is $v = 65$m/s and the chord length normal to the leading edge is $c = 1.2$m, resulting in a Reynolds number of $Re = 5.186 \cdot 10^6$. Forcing has been applied with a stochastic source generated with FRPM from RANS CFD data. The goal here is to completely impose the sound source, i.e. using the relaxation source term to prescribe a deterministic noise source.

The CFD simulations were conducted using the DLR code TAU, version 2011.1.0. TAU is a finite volume CFD code. For turbulence closure the two equation SST model is applied. The code option 'Roe2nd' is used, i.e. a second order accurate discretization of the turbulence equations is realized, and the production to destruction ratio of the turbulence kinetic energy (TKE) is limited to 20 in order to avoid spots of spuriously enhanced turbulent kinetic energy at the stagnation point of the main element. The stochastic turbulent sound sources depend strongly on the quality of the CFD simulation since their amplitude is calculated from the TKE level. For this reason, a sufficiently high resolution of the CFD mesh is necessary. In former work it could be shown that quadrilateral dominant CFD meshes produce in terms of resolution of gradients in TKE results superior to triangle dominated meshes. This feature has been accomplished using the SOLAR mesh generator. To assure a sufficient mesh resolution, the CFD grids were refined in the slat cove area. The whole CFD mesh consists of 670k points. Periodic boundary conditions are applied at the spanwise boundaries.

A block structured 2-D CAA grid is generated to resolve frequencies of up to 15 kHz in the far field. Details of the CAA mesh are shown in Fig. 23. It consists of 633k points distributed to 54 blocks. The mesh represents a leading edge normal cut through the high-lift wing. It was demonstrated in previous work[26] that 2-D CAA simulation can reveal a spectrum shape that corresponds to measurements. However, a 2-D to 3-D level calibration must be applied once to correct for absolute levels (the correction is not frequency dependent).

The mean flow which provides the propagation properties of the acoustic waves is interpolated from the RANS mesh onto the CAA mesh. The mesh is refined in the source region around the slat. The characteristic size of a vortex sound source to be resolved on the mesh is estimated to scale with respect to the smallest acoustic wave number times the local Mach number M. Hence, the grid spacing is refined to be of the order $M\Delta x$ compared to the necessary far-field spacing Δx. It determines the maximal possible non-dimensional time step of PIANO which is 2.3e-4 for the current simulation at 65m/s flow velocity. The reference time used for non-dimensionalization is defined by $t_{ref} = c_\infty/l_{ref}$, where c_∞ denotes the reference speed of sound and the reference length is chosen as the retracted chord length $l_{ref} = 1.2$ m. To improve numerical stability with explicit time integration, the used non-dimensional time step is reduced to 2.e-4.

Figs. 26(b) and 27(b) show the sound field generated by the relaxation source term. For Fig. 26(b) the relaxation parameter was directly taken from the RANS eddy viscosity, refer to Fig. 26(a) which shows the corresponding FRPM source patch where stochastic turbulence is generated with the distribution of eddy viscosity. For Fig. 27(b) a relaxation parameter defined by

$$\sigma = \hat{\sigma} \tanh(\alpha d_w) \tag{65}$$

has been used, where d_w denotes the wall-distance provided by the precursor RANS simulation, and α is a scaling parameter. Hence, essentially a constant weighting is applied, which reduces to zero in a small layer close to solid walls. The source patch, which is also geometrically slightly modified, is shown in Fig. 27(a). The variance of the stochastic fluctuations is reduced to zero at the downstream boundary of all source patches. A proper control of the induced vorticity should result in the removal of all vorticity in the solution downstream of the source patch. The pressure fluctuations present in Fig. 26(b) reveal that the first relaxation parameter cannot control the vorticity levels sufficiently, i.e. vorticity is present above the main element. For Fig. 27(b) effective control is achieved as no vorticity is visible.

A comparison of simulated and measured spectra with a standard CAA simulation technique based on Acoustic Perturbation Equations (APE) and FRPM forcing, i.e. realizing a fully deterministic noise source model, is presented in Fig. 26(a). The CAA simulations are carried out with the PIANO code (red solid line) as well with the discontinuous Galerkin code DISCO of DLR (blue line). A fairly good agreement with the measurement (black line) is obtained for frequencies up to $3kHz$. The spectra are evaluated at an observer position at $270°$ polar arc, i.e. underneath the slat. Also, the maximum of the spectrum and the low frequency shape are well reproduced. For the stochastic forcing, two source options are available, refer to the discussion in Ref.[26] Either fluctuating vorticity is modeled directly (referred to as 'model B'), or fluctuating velocity is generated, from which vorticity derives via differentiation (model A). Therefore, the vorticity from model A is solenoidal, whereas this is not guaranteed with model B. Fig. 26(b) shows results with relaxation source term and the LEE (red curve). A too steep decay is obtained. However, with an additional +3dB/octave correction towards higher frequencies, a very good agreement with the measurement (black curve) would be achievable (blue curve). Note, the additional differentiation applied in model A but not in model B could provide a mechanism that realizes the necessary shift in slope.

Spectra for forced eddy simulation with model A are shown in Fig. 27. Fig. 27(a) shows a very good agreement of the simulated spectrum (red curve) with the measurement. The simulation parameters used are $\sigma = 0.00085$ and $l = 0.0085$. The source patch with wall distant weighting is applied. Fig. 27(b) shows the effect of parameter variations on the spectrum. Besides the previous case (orange solid line), the length scale was increased to $l = 0.0135$ (green curve) and in addition the weighting factor was increased to $\sigma = 0.00125$ (magenta curve). The increase of length scale yields a slightly steeper decay of the spectrum in the high frequency regime. The increase in weighting in general causes an upward shift of the spectrum, especially in the low frequency regime.

V. Summary and Conclusions

In this paper a new way to couple a vortex-force source term to linear and non-linear perturbation equations is studied. A new relaxation formulation is proposed, that accomplishes some essential key features for successful aeroacoustic simulation with linear and non-linear perturbation equations forced by 4-D spatio-temporal synthetic turbulence, viz: i) the source term operates both, as a production and a dissipation term to control excited vorticity levels in the simulation - especially the dissipation of vorticity that is not possible to control alone with a production source terms in governing perturbation equations that include the simulation of vortex transport. Furthermore, ii) the source term only acts on the vorticity mode, i.e. no dissipative effect is introduced by the dissipation source term for the simulation of acoustic modes. Finally, iii) the source term acts wave-number selective in a way that high wave-number components of the simulated vorticity dynamics are closely prescribed by the fluctuating vorticity field, whereas low wave-number components can freely develop. That way it becomes possible to modify the datum CAA simulation technique with deterministic source term from stochastic models, i.e. all vortex dynamics are entirely prescribed by the right-hand side vortex sound source, towards partly scale resolved simulation, where the dynamics of the resolved scales is simulated while the contribution of smaller scales onto the larger scales (i.e. the back scattering of energy) is accomplished by the relaxation source term. That way the gap is bridged between scale resolving simulation, such as LES or DNS, and RANS based fully deterministic noise source modeling. The coupling strength is determined by the relaxation parameter. For a large parameter, the vortex dynamics are entirely imposed by the source model (deterministic mode), whereas with vanishing parameter scale resolving simulation becomes feasible. For the latter purpose, Non-linear perturbation equations (NLPE) have been derived that enable a scale resolving simulation mode.

It was successfully demonstrated that the relaxation source term allows to control vorticity levels without significantly affecting acoustic propagation. In particular, the suppression of hydrodynamic instabilities in the unstable jet problem of the 4th CAA Workshop on Benchmark Problems without disturbing acoustic radiation and refraction was demonstrated. In a test problem with fluctuations imposed by the relaxation source term from stochastically generated turbulence, the all-pass characteristic derived theoretically was verified. Test simulations with strong coupled relaxation source term (deterministic mode) reveal good reproduction of the broadband sound characteristics for a high-lift test case.

Acknowledgments

Appendix

A. Excited frequency spectrum

The vorticity spectrum used in section C is the wave-number-frequency Fourier transform of the vorticity two-point cross-correlation function,

$$\Phi\left(\boldsymbol{k},\omega\right) = \mathcal{F}\left(R(\boldsymbol{r},\tau)\right), \tag{66}$$

with the space-time Fourier transform as defined by Eqs. (10) and (11). This gives

$$\Phi\left(\boldsymbol{k},\omega\right) = \frac{1}{(2\pi)^n} \iint R(\boldsymbol{r},\tau)\exp\left(i\left(\omega\tau - \boldsymbol{kr}\right)\right)\mathrm{d}^n\boldsymbol{r}\mathrm{d}\tau \tag{67}$$

For stationary turbulence the two-point cross-correlation function of quantity $q(\boldsymbol{x},t)$ follows from the time average

$$R(\boldsymbol{r},\tau) = \lim_{T\to\infty}\frac{1}{T}\int_{t_0}^{t_0+T} q(\boldsymbol{x},t)q(\boldsymbol{x}+\boldsymbol{r},t+\tau)\mathrm{d}t. \tag{68}$$
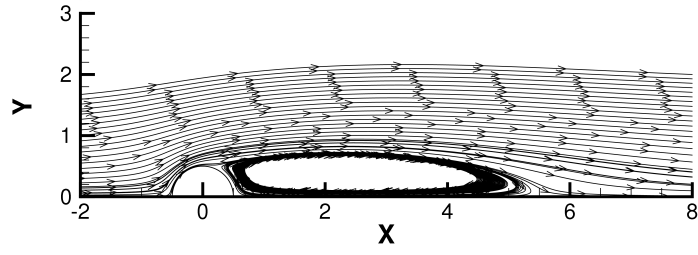
(a) Re=150, M= 0.1.
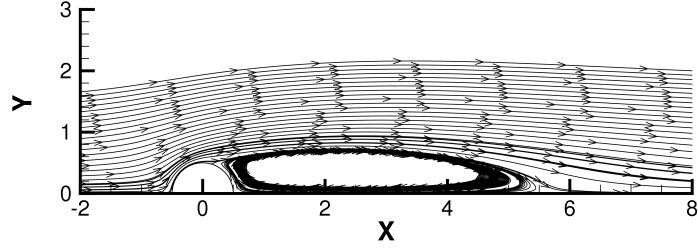
(b) Re=150, M= 0.2.
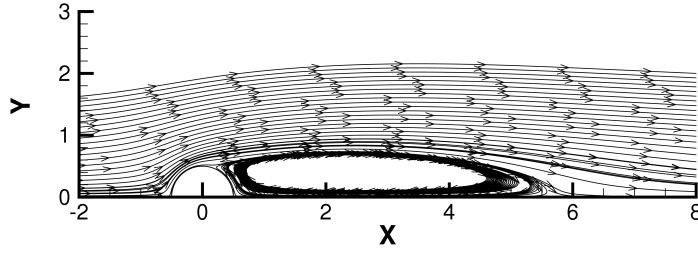
(c) Re=150, M= 0.3.

Figure 4. RANS mean-flow velocity streamlines for different Mach numbers involving a splitter plate at $y = 0$ to suppress the onset of laminar vortex shedding in the RANS simulation.

For homogeneous turbulence assumed here the cross-correlation function does not depend on position $\boldsymbol{x}$. Hence, without harm we can further average the resulting cross-correlation function over space, i.e.

$$R(\boldsymbol{r}, \tau) = \lim_{T,V \to \infty} \frac{1}{VT} \int_V \int_{t_0}^{t_0+T} q(\boldsymbol{x}, t) q(\boldsymbol{x}+\boldsymbol{r}, t+\tau) \mathrm{d}t \mathrm{d}^n \boldsymbol{x}. \tag{69}$$

Both quantities under the latter integral can be expressed by their Fourier transforms,

$$q(\boldsymbol{x}, t) = \frac{1}{2\pi} \iint \hat{q}(\boldsymbol{k}_1, \omega_1) \exp\left(-i\left(\omega_1 t - \boldsymbol{k}_1 \boldsymbol{x}\right)\right) \mathrm{d}^n \boldsymbol{k}_1 \mathrm{d}\omega_1, \tag{70}$$

$$q(\boldsymbol{x}+\boldsymbol{r}, t+\tau) = \frac{1}{2\pi} \iint \hat{q}(\boldsymbol{k}_2, \omega_2) \exp\left(-i\left(\omega_2 t - \boldsymbol{k}_2 \boldsymbol{x}\right)\right)$$
$$\times \exp\left(-i\left(\omega_2 \tau - \boldsymbol{k}_2 \boldsymbol{r}\right)\right) \mathrm{d}^n \boldsymbol{k}_2 \mathrm{d}\omega_2. \tag{71}$$

By inserting Eq. (69) with quantities q substituted from Eqs. (70) and (71) into Eq. (67) an expression for the wave-number-frequency spectrum in terms of the wave-number-frequency Fourier transforms of q is obtained, viz.

$$\Phi\left(\boldsymbol{k}, \omega\right) = \lim_{T,V \to \infty} \frac{1}{VT} \frac{1}{(2\pi)^{n+2}} \iiiiiiii \hat{q}\left(\boldsymbol{k}_1, \omega_1\right) \hat{q}\left(\boldsymbol{k}_2, \omega_2\right) \exp\left[-i\left(\left(\omega_1 + \omega_2\right)t - \left(\boldsymbol{k}_1 + \boldsymbol{k}_2\right)\boldsymbol{x}\right)\right]$$
$$\times \exp\left[-i\left(\left(\omega_2 - \omega\right)\tau - \left(\boldsymbol{k}_2 - \boldsymbol{k}\right)\boldsymbol{r}\right)\right] \mathrm{d}t \, \mathrm{d}^n \boldsymbol{x} \, \mathrm{d}^n \boldsymbol{k}_2 \, \mathrm{d}\omega_2 \, \mathrm{d}^n \boldsymbol{r} \, \mathrm{d}\tau \, \mathrm{d}^n \boldsymbol{k}_1 \, \mathrm{d}\omega_1. \tag{72}$$

American Institute of Aeronautics and Astronautics

Integration with respect to t yields $2\pi\delta\left(\omega_1 + \omega_2\right)$. Integration with respect to $\boldsymbol{x}$ yields $(2\pi)^n\,\delta\left(\boldsymbol{k}_1 + \boldsymbol{k}_2\right)$. Eventually, integration with respect to $\boldsymbol{k}_2$ and ω_2 provides

$$\Phi\left(\boldsymbol{k}, \omega\right) = \lim_{T,V\to\infty} \frac{1}{VT}\frac{1}{2\pi} \iiiint \hat{q}\left(\boldsymbol{k}_1, \omega_1\right)\hat{q}^*\left(\boldsymbol{k}_1, \omega_1\right)\exp\left[i\left((\omega_1 + \omega)\tau - (\boldsymbol{k}_1 + \boldsymbol{k})\,\boldsymbol{r}\right)\right]\mathrm{d}^n\boldsymbol{r}\,\mathrm{d}\tau\,\mathrm{d}^n\boldsymbol{k}_1\,\mathrm{d}\omega_1. \tag{73}$$

Here the asterisk indicates the conjugate complex of the combined space-time Fourier transform, given by $\hat{q}^*(\boldsymbol{k}_1, \omega_1) = \hat{q}(-\boldsymbol{k}_1, -\omega_1)$. Next, integration with respect to τ and $\boldsymbol{r}$ yields $2\pi\delta(\omega_1 + \omega)$ and $(2\pi)^n\,\delta\left(\boldsymbol{k}_1 + \boldsymbol{k}\right)$, respectively. Finally, the integration with respect to $\boldsymbol{k}_1$ and ω_1 provides

$$\Phi\left(\boldsymbol{k}, \omega\right) = \lim_{T,V\to\infty} \frac{(2\pi)^n}{VT}\left\{\hat{q}\left(\boldsymbol{k}, \omega\right)\hat{q}^*\left(\boldsymbol{k}, \omega\right)\right\} = \lim_{T,V\to\infty} \frac{(2\pi)^n}{VT}\left|\hat{q}\left(\boldsymbol{k}, \omega\right)\right|^2. \tag{74}$$

In section C the relationship between the wave-number-frequency Fourier transforms of forced and reference vorticity

$$\hat{\Omega}_3' = T(\boldsymbol{k}, \omega)\hat{\Omega}_3^{ref} \tag{75}$$

was derived, where $T(\omega)$ represents the complex transfer function between both quantities. Since two complex quantities obey the relationship $|z_1 z_2|^2 = |z_1|^2|z_2|^2$, it follows from Eq. (74) that the subsequent relationship between forced and reference wave-number-frequency spectra must hold:

$$\Phi\left(\boldsymbol{k}, \omega\right) = \left|T\left(\boldsymbol{k}, \omega\right)\right|^2 \Phi^{ref}\left(\boldsymbol{k}, \omega\right). \tag{76}$$

B. Model spectrum

A simplified 2-D two-point cross-correlation function of fluctuating vorticity is used to study the behavior of the relaxation source term, which is defines a Gaussian spatial correlation function and assumes frozen turbulence of turbulent length scale l and variance $\hat{R}$. That is,

$$R(\boldsymbol{x}, \tau) = \hat{R}\exp\left[-\frac{\ln(2)}{l^2}\left(\left(x_1 - v_1^0\tau\right)^2 + x_2^2\right)\right]. \tag{77}$$

The wave-number-frequency spectrum related to this function, which is used as a reference solution in the relaxation model, is given by Eq. (10). Hence, the integrals to be solved read

$$\Phi^{ref}\left(\boldsymbol{k}, \omega\right) = \frac{1}{(2\pi)^2}\iint \hat{R}\exp\left[-\frac{\ln(2)}{l^2}\left(\left(x_1 - v_1^0\tau\right)^2 + x_2^2\right)\right]\exp\left(i\left(\omega\tau - \boldsymbol{k}\boldsymbol{x}\right)\right)\mathrm{d}^n\boldsymbol{x}\mathrm{d}\tau \tag{78}$$

The first step is the integration with respect to x_1. The integral is

$$I_1 = \int_{-\infty}^{\infty}\exp\left[-\frac{\ln(2)}{l^2}(x_1 - v_1^0\tau)^2\right]\exp\left[-ik_1 x_1\right]\mathrm{d}x_1. \tag{79}$$

This yields

$$I_1 = l\sqrt{\frac{\pi}{\ln(2)}}\exp\left[-\frac{k_1^2 l^2}{4\ln(2)}\right]\exp\left[-i\alpha_1 v_1^0\tau\right]. \tag{80}$$

The second step is the integration with respect to τ. The integral to be solved reads

$$I_2 = \int_{-\infty}^{\infty}\exp\left[i\left(\omega - \alpha_1 v_1^0\right)\tau\right]\mathrm{d}\tau, \tag{81}$$

which readily gives

$$I_2 = 2\pi\delta\left(\omega - \alpha_1 v_1^0\right). \tag{82}$$

The final integral with respect to x_2 gives

$$\iint_{-\infty}^{\infty}\exp\left[-\frac{\ln(2)}{l^2}x_2^2\right]\mathrm{d}x_2 = \sqrt{\frac{\pi}{\ln(2)}}l\exp\left[-\frac{k_2^2 l^2}{4\ln(2)}\right]. \tag{83}$$

Altogether, the wavenumber-frequency spectrum associated to the cross-correlation model Eq. (77) becomes (with $k^2 = k_1^2 + k_2^2$)

$$\Phi^{ref}\left(\boldsymbol{k}, \omega\right) = \frac{\hat{R}l^2}{2\ln(2)}\exp\left(-\frac{k^2 l^2}{4\ln(2)}\right)\delta\left(\omega - k_1 v_1^0\right). \tag{84}$$

American Institute of Aeronautics and Astronautics

C. Forced frequency spectrum

The model problem studied in section C is

$$\frac{\partial \Omega_3'}{\partial t} + v_1^0 \frac{\partial \Omega_3'}{\partial x_1} = \sigma \left(\frac{\partial^2 \Omega_3'}{\partial x_i^2} - \frac{\partial^2 \Omega_3^{ref}}{\partial x_i^2} \right). \tag{85}$$

The wave-number-frequency spectrum that results from the forcing with relaxation source term is given by Eq. (76) with the transfer function defined by Eq. (14) and using the reference wave-number-frequency spectrum Eq. (84) from the previous paragraph. The corresponding frequency spectrum is given by the integration of the wave-number-frequency spectrum over all $\boldsymbol{k}$, refer to Eq. (19). That is,

$$S(\omega) = \frac{\hat{R}l^2}{2\ln(2)} \iint \frac{\sigma^2 (k_1^2 + k_2^2)^2}{\sigma^2 (k_1^2 + k_2^2)^2 + (\omega - k_1 v_1^0)^2} \exp\left(-\frac{(k_1^2 + k_2^2)\, l^2}{4\ln(2)} \right) \delta\left(\omega - k_1 v_1^0 \right) \mathrm{d}k_1 \mathrm{d}k_2 \tag{86}$$

Integration with respect to k_1 yields

$$S(\omega) = \frac{\hat{R}l^2}{2\ln(2)|v_1^0|} \int \frac{\sigma^2 \left(\left(\frac{\omega}{v_1^0}\right)^2 + k_2^2 \right)^2}{\sigma^2 \left(\left(\frac{\omega}{v_1^0}\right)^2 + k_2^2 \right)^2 + \left(\omega - \frac{\omega}{v_1^0} v_1^0 \right)^2} \exp\left(-\frac{\left(\left(\frac{\omega}{v_1^0}\right)^2 + k_2^2 \right) l^2}{4\ln(2)} \right) \mathrm{d}k_2 \tag{87}$$

The second summand in the denominator vanishes and thus the whole fraction term reduces to unity. The final k_2-integration yields the forced frequency spectrum

$$S(\omega) = \sqrt{\frac{\pi}{\ln(2)}} \frac{\hat{R}l}{|v_1^0|} \exp\left(-\frac{\omega^2 l^2}{4\ln(2)(v_1^0)^2} \right). \tag{88}$$

The forced frequency spectrum exactly corresponds to the reference spectrum, Eq. (20).

References

[1] Ewert, R. and Schröder, W., "Acoustic Perturbation Equations Based on Flow Decomposition via Source Filtering," *J. Comput. Phys.*, Vol. 188, 2003, pp. 365–398.

[2] Schneider, K., Farge, M., Pellegrino, G., and M.Rogerss, M., "Coherent vortex simulation of three-dimensional turbulent mixing layers using orthogonal wavelets," *Physics of Fluids*, Vol. 534, 2005, pp. 3966.

[3] Farge, M., Schneider, K., and Kevlahan, N., "Non-Gaussianity and coherent vortex simulation for two-dimensional turbulence using an adaptive othogonal wavelet basis," *Physics of Fluids*, Vol. 11(8), 1999, pp. 2187–2201.

[4] Farge, M. and Schneider, K., "Coherent Vortex Simulation (CVS), A Semi-Deterministic Turbulence Model Using Wavelets," *Turbulence and Combustion*, Vol. 66, 2001, pp. 393–426.

[5] Batten, P., Ribaldone, E., Casella, M., and Chakravarthy, S., "Towards a generalized non-linear acoustics solver," *AIAA Pap. AIAA 2004-3001*, 2004.

[6] Ewert, R., Dierke, J., Siebert, J., Neifeld, A., Appel, C., Siefert, M., and Kornow, O., "CAA broadband noise prediction for aeroacoustic design," *Journal of Sound and Vibration*, Vol. 330, No. 17, 2011.

[7] Ewert, R., "Broadband slat noise prediction based on CAA and stochastic sound sources from a fast random particle-mesh (RPM) method," *Computers & Fluids*, Vol. 37, 2008, pp. 369–387.

[8] Ewert, R., "RPM - the fast Random Particle-Mesh method to realize unsteady turbulent sound sources and velocity fields for CAA applications," *AIAA Pap. 2007-3506*, 2007.

[9] Morris, P. J. and Agarwal, A., "Problem 1 - Radiation and refraction of sound waves through a two-dimensional shear layer," *Fourth Computational Aeroacoustics (CAA) Workshop on Benchmark Problems*, No. CP–2004-212954, NASA Glenn Research Center, September 2004.

[10] Ewert, R., Dierke, J., Appel, C., and Herr, M., "RANS/CAA based prediction of NACA 0012 broadband trailing edge noise and experimental validation," *15th AIAA/CEAS Aeroacoustics Conference, Miami, Florida, USA*, 2009, AIAA Pap. 2009-3269.

[11] Freund, J. B., "A Simple Method for Computing Far-Field Sound in Aeroacoustic Computations," *Journal of Computational Physics*, Vol. 157, 2000, pp. 796–800.

[12] Lighthill, M. J., "On Sound Generated Aerodynamically: I. General Theory," *Proc. R. Soc. London Ser. A*, Vol. 211, 1952, pp. 564–587.

[13] Tam, C. and Webb, J., "Dispersion-Relation-Preserving Finite Difference Schemes for Computational Acoustics," *Journal of Computational Physics*, Vol. 107, 1993, pp. 262–281.

[14] Dantinne, G., Jeanmart, H., Winckelmans, G., Legat, V., and Carati, D., "Hyperviscosity and Vorticity-Based Models for Subgrid Scale Modeling," *Applied Scientific Research*, Vol. 59, 1998, pp. 409–420.

[15]Delfs, J., Bauer, M., Ewert, R., Grogger, H., Lummer, M., and Lauke, T., *Numerical simulation of aerodynamic noise with DLR's aeroacoustic code PIANO - PIANO manual version 5.2*, Braunschweig, Germany, 2007.

[16]Akkermans, R., Ewert, R., Moghadam, S., Dierke, J., and Buchmann, N., "Towards Overset LES Prediction of Sound Sources," *Notes on Numerical Fluid Mechanics and Multidisciplinary design, Advances on Hybrid RANS-LES Modelling*, 5th Symposium on Hybrid RANS-LES Methods, 2014, submitted.

[17]Long, L. N., "A nonconservative nonlinear flowfield splitting method for 3-D unsteady fluid dynamics," *AIAA Pap. 2000-1998*, 2000.

[18]Morris, P., Long, L., Bangalore, A., and Wang, Q., "A parallel three-dimensional computational aeroacoustics method using nonlinear disturbance equations," *Journal of Computational Physics*, Vol. 133, 1997, pp. 56–74.

[19]Liu, J. and Long, L., "Direct aeroacoustic and aerodynamic simulation of multi-hole engine liners using the non-linear disturbance equations," *AIAA Pap. 98-2320*, 1998.

[20]Terracol, M., "A zonal RANS/LES approach for noise source prediction," *Flow Turbulence Combust.*, Vol. 77, 2006, pp. 161–184.

[21]Manoha, E., Terracol, M., Lemoine, B., Griffon, I. L., and Garrec, T. L., "Slat noise measurement and numerical prediction in the VALIANT programme." *AIAA Pap. 2012-2100*, 2012.

[22]Tam, C. K. and Kurbatski, K., "Microfluid Dynamics and Acoustics of Resonant Liners," *AIAA Journal*, Vol. 38, No. 8, 2000, pp. 1331–1339.

[23]Tam, C., Kurbatski, K., Ahuja, K., and Jr., R. G., "A numerical and experimental investigation of the dissipation mechanism of resonant acoustic liners," *Journal of Sound and Vibration*, Vol. 245, No. 3, 2001, pp. 545–557.

[24]Tam, C. K. and Ju, H., "Airfoil tones at moderate Reynolds number," *Journal of Fluid Mechanics*, Vol. 690, 2011, pp. 536–570.

[25]Inoue, O. and Hatakeyama, N., "Sound generation by a two-dimensional circular cylinder in a uniform flow," *Journal of Fluid Mechanics*, Vol. 471, 2002, pp. 285–314.

[26]Ewert, R., Dierke, J., Appel, C., Pott-Pollenske, M., and Sutcliff, M., "CAA-RPM Prediction and Validation of Slat Setting Influence on Broadband High-Lift Noise Generation," *16th AIAA/CEAS Aeroacoustics Conference, Stockholm, Sweden*, 2010, AIAA Pap. 2010-3833.
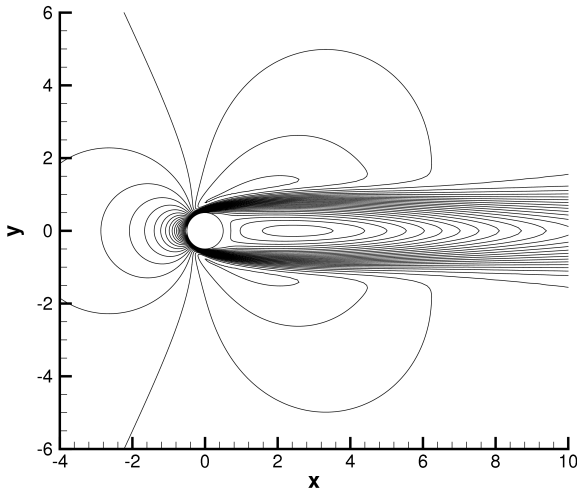
(a) Base flow x-velocity v^0 from TAU RANS.
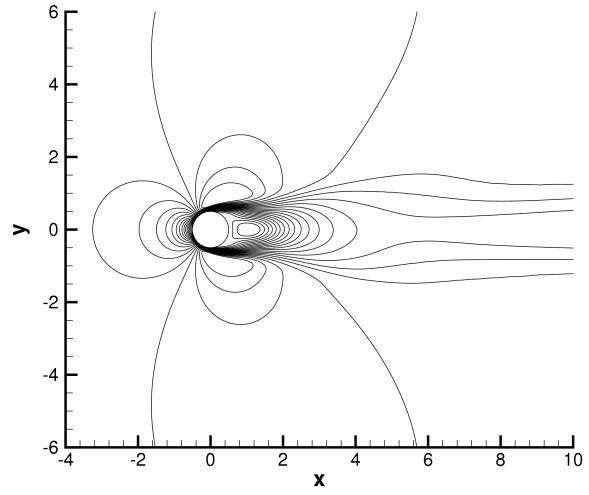
(b) Mean x-velocity $v^0 + \overline{v'}$ with added mean contribution from PIANO.

Figure 5. Schematic view of base and mean-flow contour lines for circular cylinder simulation in M = 0.2.
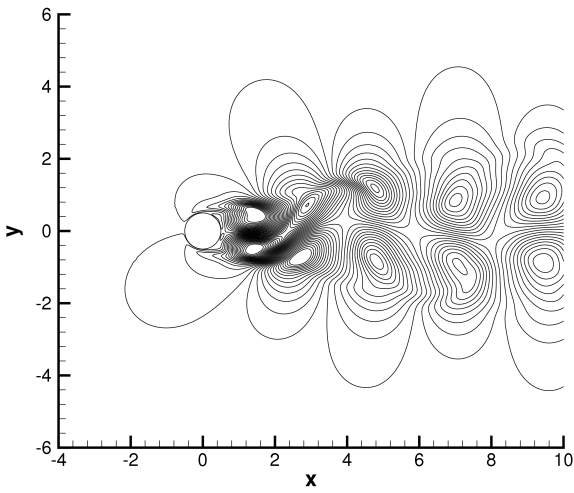
(a) Fluctuating x-velocity $v' - \overline{v'}$.
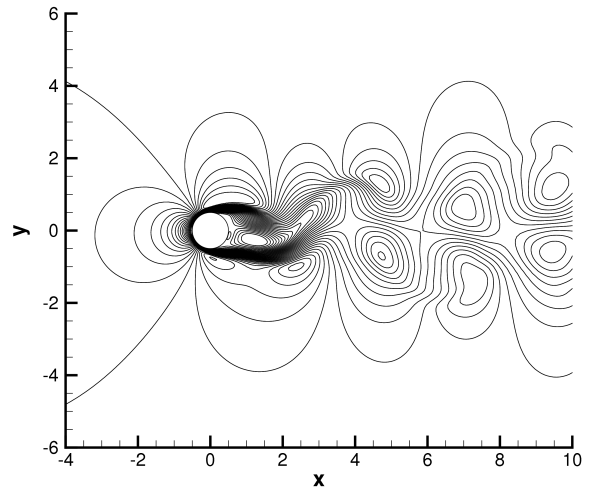
(b) Total x-velocity $v^0 + v'$.

Figure 6. Schematic view of fluctuating and total-flow contour lines for circular cylinder simulation in M = 0.2.

American Institute of Aeronautics and Astronautics
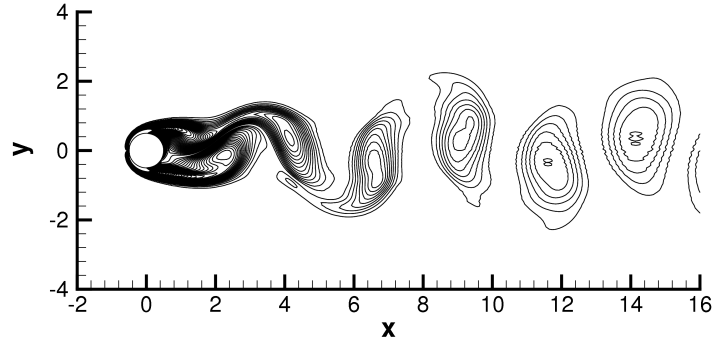
Figure 7. Spatial development of a vorticity field for M = 0.1, Re = 150. The contour levels are from $\Omega_{min} = $ -0.75 to $\Omega_{max} = +0.75$ with an increment 0.015.
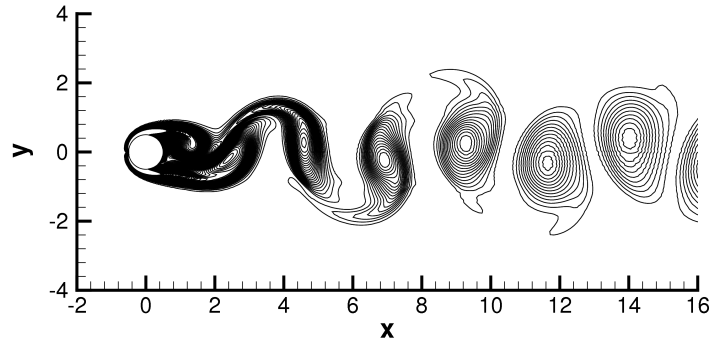
Figure 8. Spatial development of a vorticity field for M = 0.2, Re = 150. The contour levels are from $\Omega_{min} = $ -1.0 to $\Omega_{max} = +1.0$ with an increment 0.02.
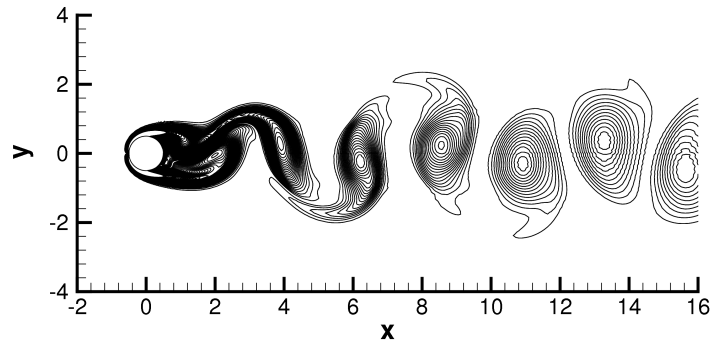
Figure 9. Spatial development of a vorticity field for M = 0.3, Re = 150. The contour levels are from $\Omega_{min} = $ -1.5 to $\Omega_{max} = +1.5$ with an increment 0.03.

American Institute of Aeronautics and Astronautics

(a) t=1710.

(b) t=1725.
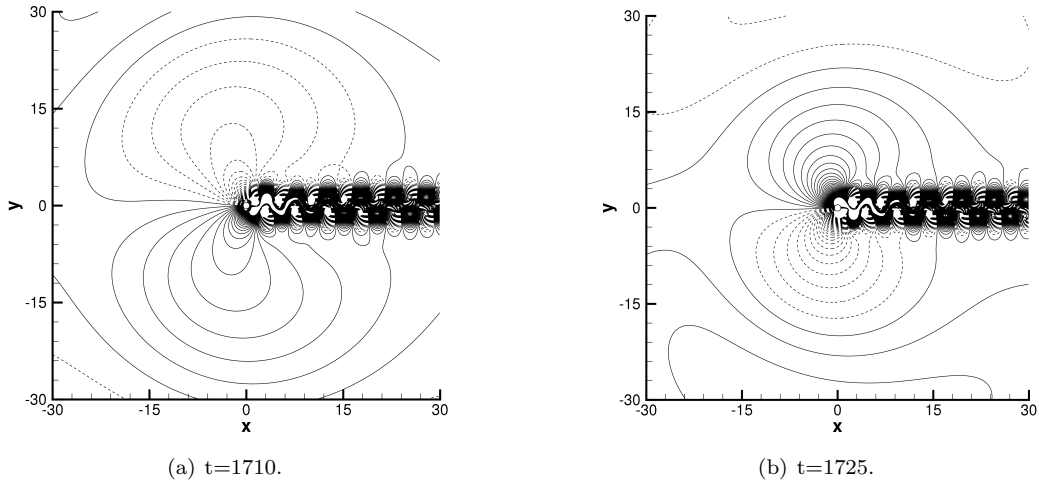
Figure 10. Time development of pressure fluctuation $\widetilde{p}'$. M = 0.1, Re = 150. The contour levels are from $\widetilde{p}' = -1.0M^{2.5}$ to $\widetilde{p}' = 1.0M^{2.5}$ with an increment $0.0025M^{2.5}$. ——, $\widetilde{p}' > 0$; − − −, $\widetilde{p}' < 0$.

(a) t=1710.

(b) t=1725.
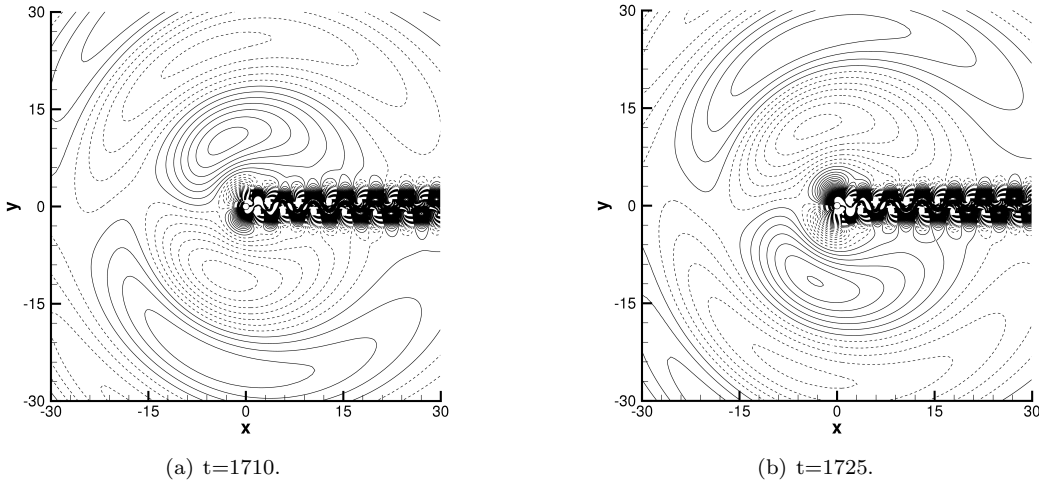
Figure 11. Time development of pressure fluctuation $\widetilde{p}'$. M = 0.2, Re = 150. The contour levels are from $\widetilde{p}' = -1.0M^{2.5}$ to $\widetilde{p}' = 1.0M^{2.5}$ with an increment $0.0025M^{2.5}$; ——, $\widetilde{p}' > 0$; − − −, $\widetilde{p}' < 0$.

(a) t=1710.

(b) t=1725.
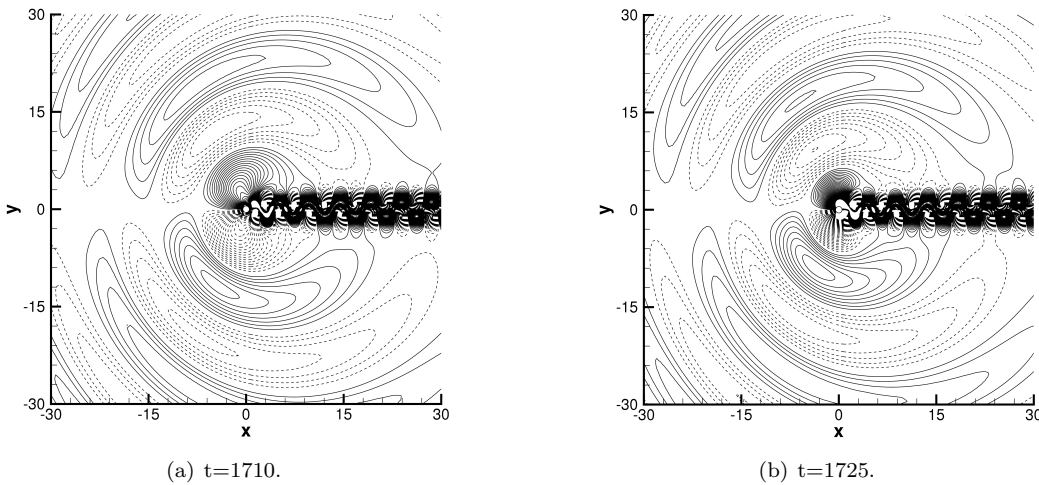
Figure 12. Time development of pressure fluctuation $\widetilde{p}'$. M = 0.3, Re = 150. The contour levels are from $\widetilde{p}' = -1.0M^{2.5}$ to $\widetilde{p}' = 1.0M^{2.5}$ with an increment $0.0025M^{2.5}$; ——, $\widetilde{p}' > 0$; − − −, $\widetilde{p}' < 0$.

American Institute of Aeronautics and Astronautics
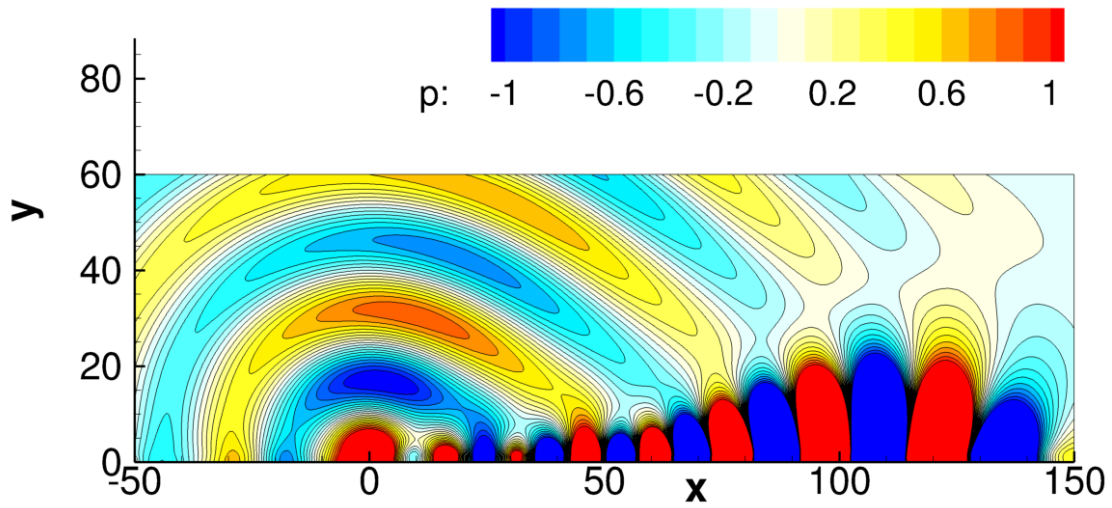
Figure 13. Unstable jet, category 4, problem 1, of the 4th CAA Workshop on Benchmark Problems,[9] 7 harmonic source cycles computed.
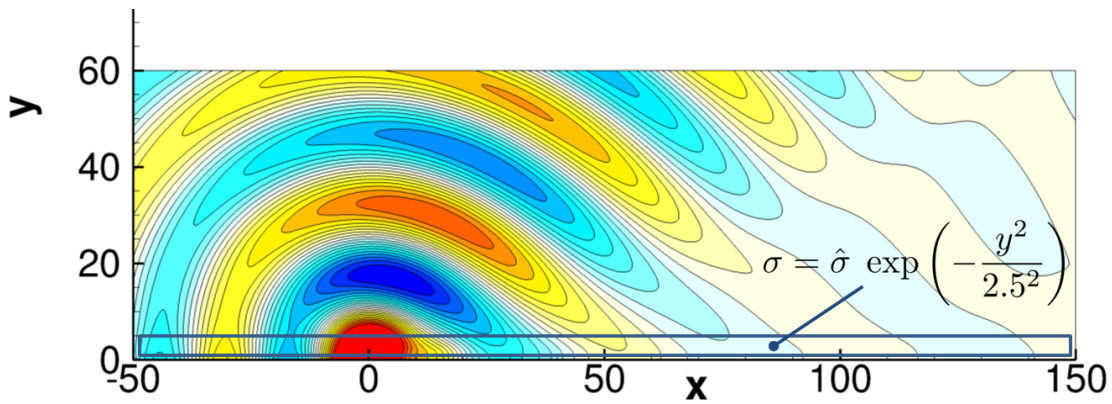
Figure 14. Relaxation source applied in indicated domain without forcing, peak amplitude $\hat{\sigma} = 0.03$, vertical scaling as indicated in the figure and according to Eq. (62).

(a) Unstable jet, $\sigma = 0$

(b) Case 1: $\hat{\sigma} = 0.01$, $x = -50 \ldots 150$, $y = 0 \ldots 5$

(c) Case 2: $\hat{\sigma} = 0.02$, $x = -50 \ldots 150$, $y = 0 \ldots 5$

(d) Case 3: $\hat{\sigma} = 0.03$, $x = -50 \ldots 150$, $y = 0 \ldots 5$

(e) Case 4: $\sigma = 0.05 = const.$, $x = -50 \ldots 150$, $y = 0 \ldots 5$

(f) Case 5: $\sigma = 0.05 = const.$, $x = -50 \ldots 150$, $y = 0 \ldots 60$

(g) Case 6: $\hat{\sigma} = 0.05$, $x = -50 \ldots 50$, $y = 0 \ldots 5$

(h) Case 7: $\hat{\sigma} = 0.1$, $x = -50 \ldots 150$, $y = 0 \ldots 5$
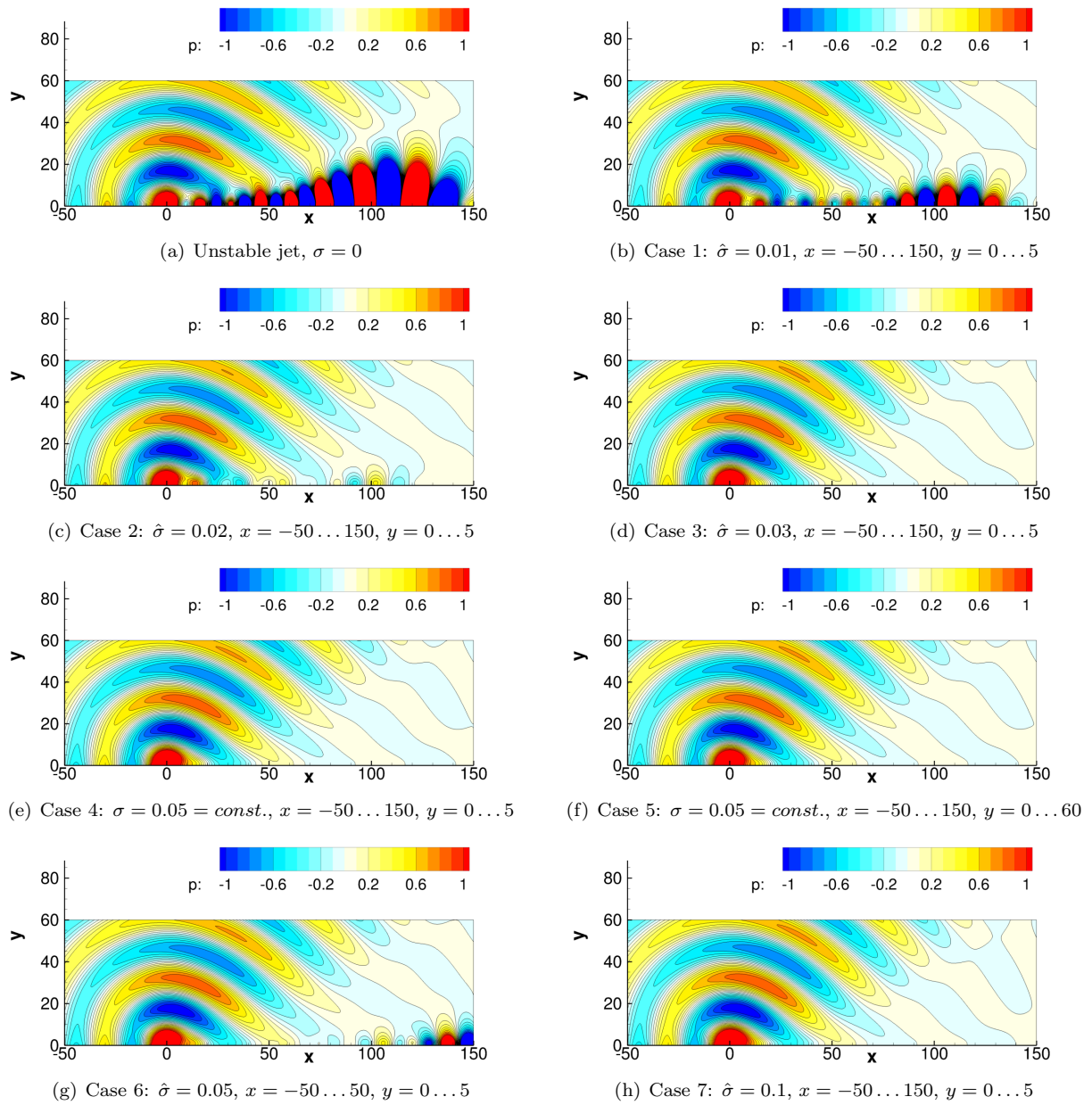
Figure 15. **Unstable jet problem and relaxation source applied without forcing; extension of domain with relaxation source term applied as indicated at the figures; σ indicates constant diffusion coefficient, $\hat{\sigma}$ peak amplitude of vertically variable weighting according to Eq. (62).**
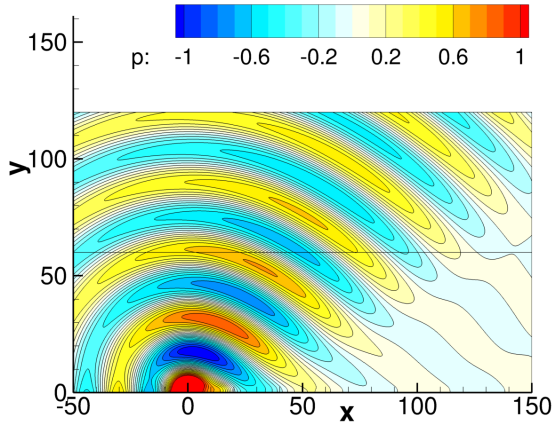
(a) Case 8: $\hat{\sigma} = 0.05$, $x = -50 \ldots 150$, $y = 0 \ldots 5$
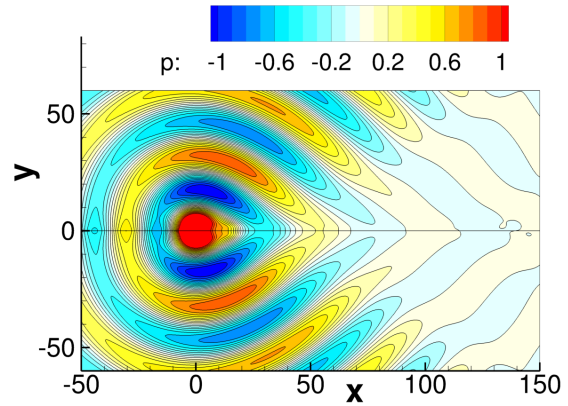
(b) Case 9: $\hat{\sigma} = 0.05$, $x = -50 \ldots 150$, $y = -5 \ldots 5$

Figure 16. **Unstable jet problem and relaxation source applied without forcing (extended CAA domains); extension of domain with relaxation source term applied as indicated at the figures; σ indicates constant diffusion coefficient, $\hat{\sigma}$ peak amplitude of vertically variable weighting according to Eq. (62).**
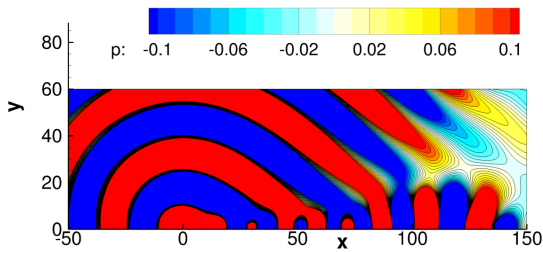
(a) Case 1: $\hat{\sigma} = 0.01$, $x = -50 \ldots 150$, $y = 0 \ldots 5$
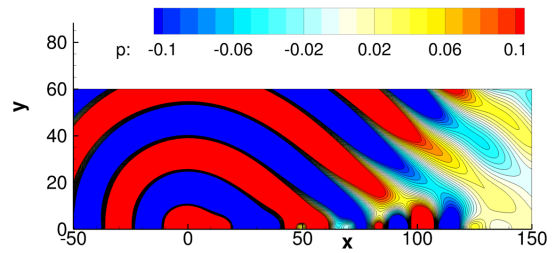
(b) Case 2: $\hat{\sigma} = 0.02$, $x = -50 \ldots 150$, $y = 0 \ldots 5$
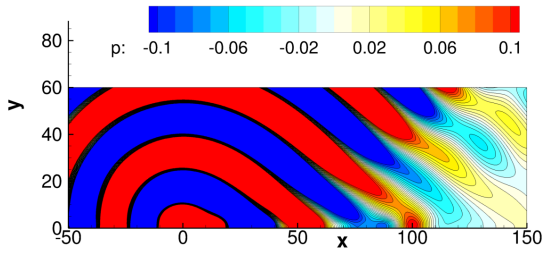
(c) Case 3: $\hat{\sigma} = 0.03$, $x = -50 \ldots 150$, $y = 0 \ldots 5$
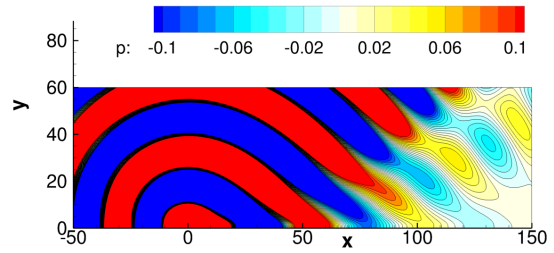
(d) Case 4: $\sigma = 0.05 = const.$, $x = -50 \ldots 150$, $y = 0 \ldots 5$
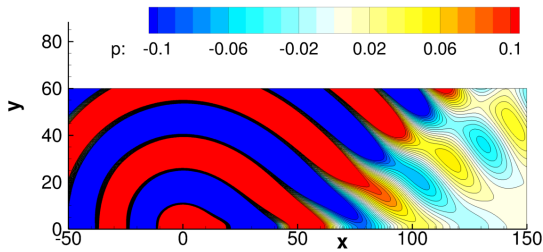
(e) Case 5: $\sigma = 0.05 = const.$, $x = -50 \ldots 150$, $y = 0 \ldots 60$
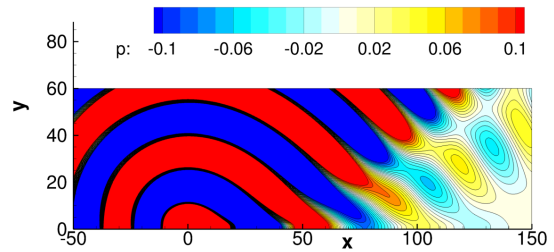
(f) Case 7: $\hat{\sigma} = 0.1$, $x = -50 \ldots 150$, $y = 0 \ldots 5$

Figure 17. **Unstable jet problem and relaxation source applied without forcing (reduced contour levels); extension of domain with relaxation source term applied as indicated at the figures; σ indicates constant diffusion coefficient, $\hat{\sigma}$ peak amplitude of vertically variable weighting according to Eq. (62).**

American Institute of Aeronautics and Astronautics

(a) $y = 15$

(b) $y = 50$
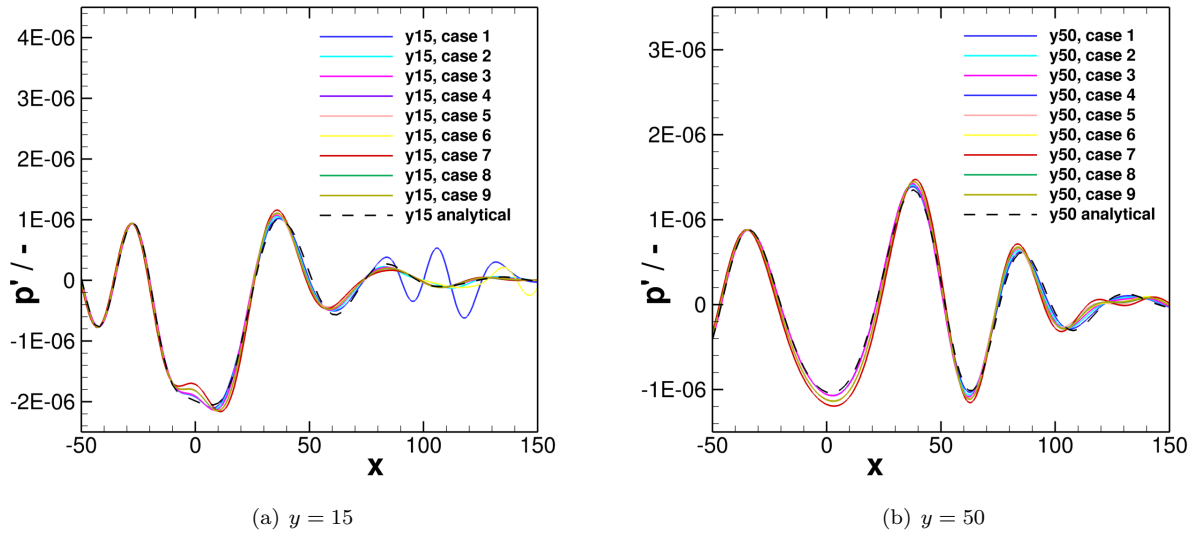
Figure 18. Pressure perturbation at the start of a cycle along two horizontal lines.

(a) Ω'_3, FRPM generated reference solution

(b) Ω'_3, CAA field
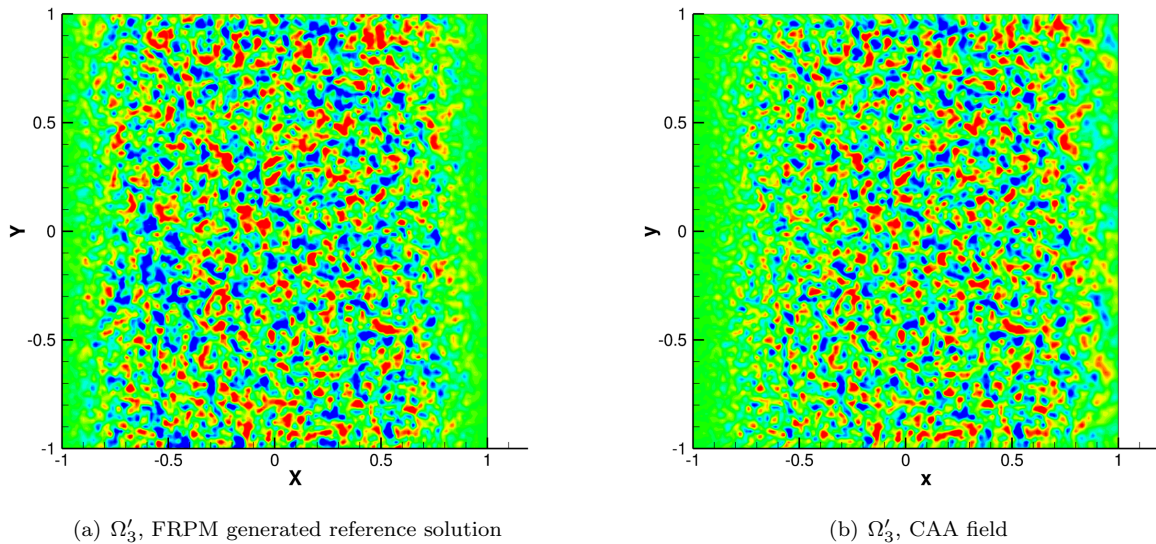
Figure 19. Snapshot of fluctuating vorticity Ω'_3, 50k time steps, FRPM generated reference solution (length scale realized $l = 0.02$), (a); field present in CAA simulation, (b); relaxation parameter $\sigma = 0.001$.
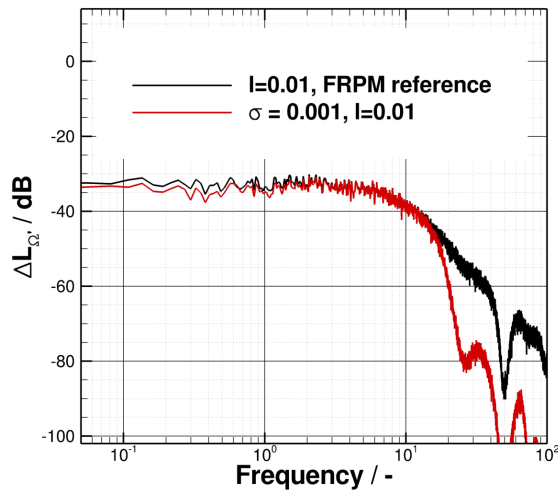
(a) Frozen Turbulence
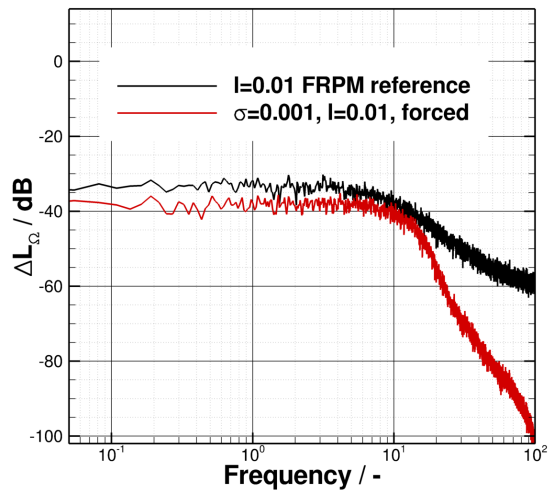
(b) Turbulent decay

Figure 20. Reference versus realized frequency spectra for sampling point $x = 0$ and $y = 0$.
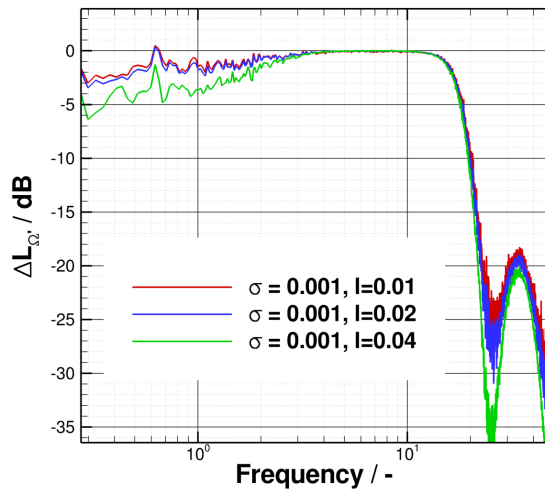
(a) Length scale variation
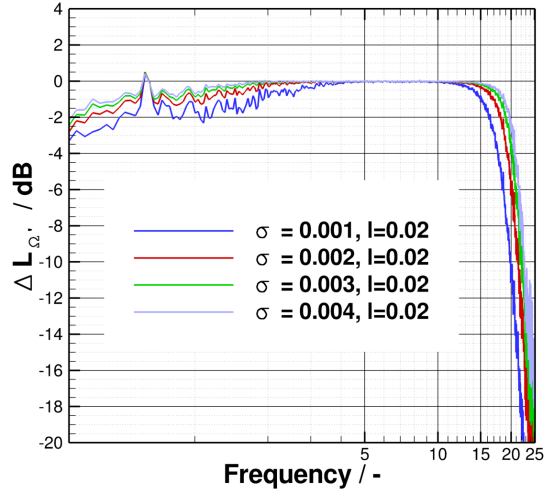
(b) Weighting variation

Figure 21. Frequency transfer function for frozen turbulence.
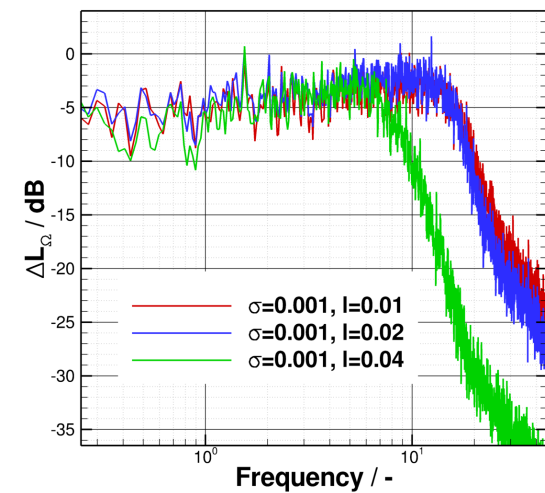
(a) Length scale variation
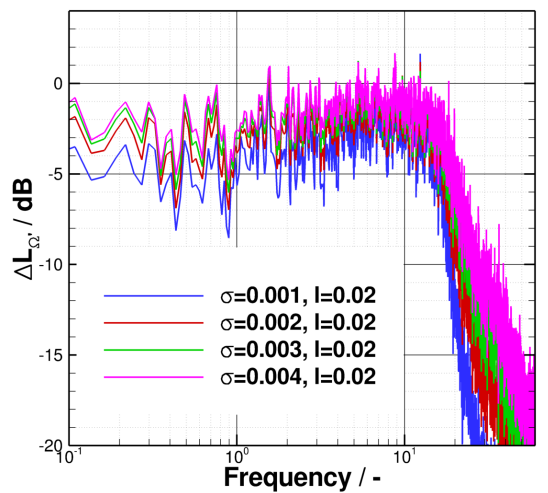
(b) Weighting variation

Figure 22. Frequency transfer function for decaying turbulence.

American Institute of Aeronautics and Astronautics
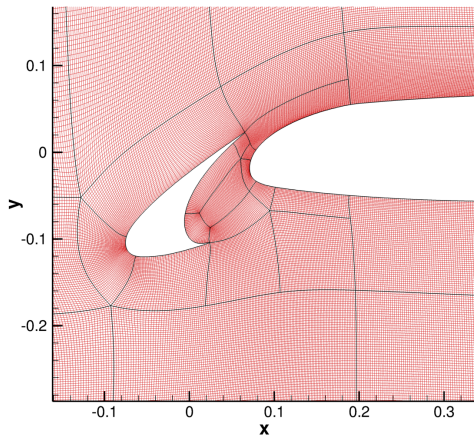
(a) Mesh around the slat
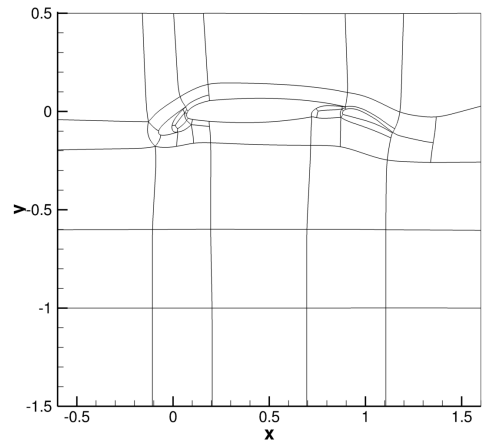
(b) CAA mesh topology

Figure 23. CAA mesh used for the high-lift test case.
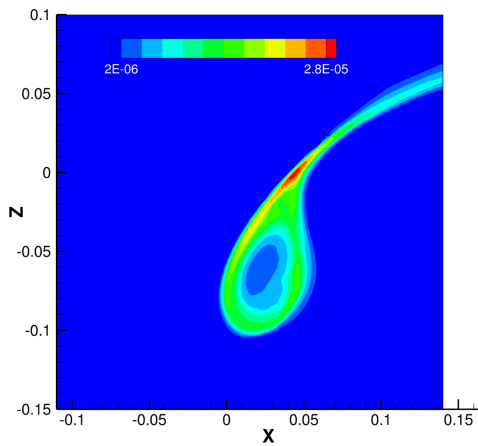
(a) Source patch with relaxation parameter scaling from RANS eddy viscosity
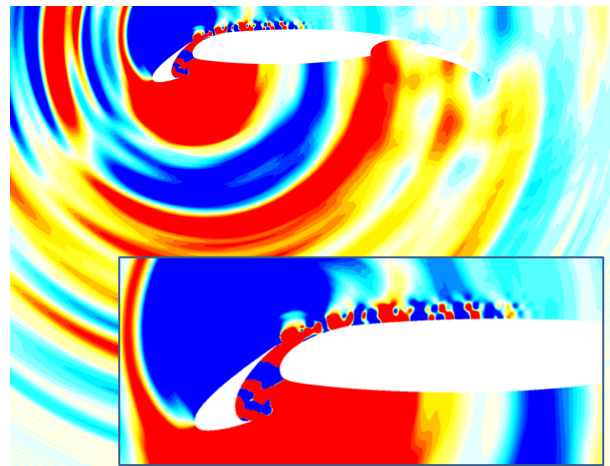
(b) Sound field

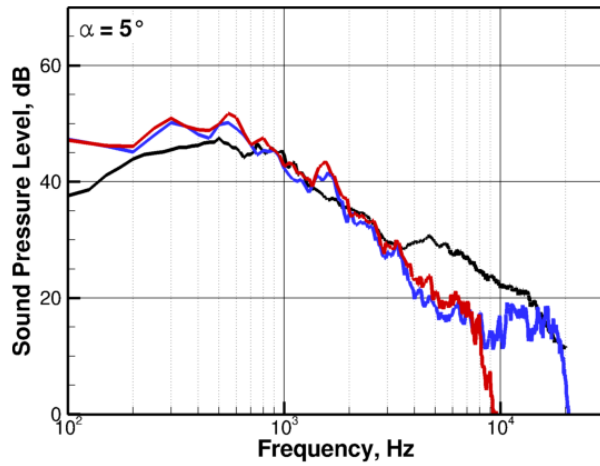**Figure 24. High-lift simulation with RANS eddy viscosity derived relaxation scaling.**
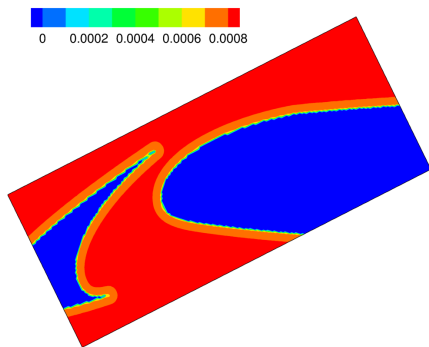
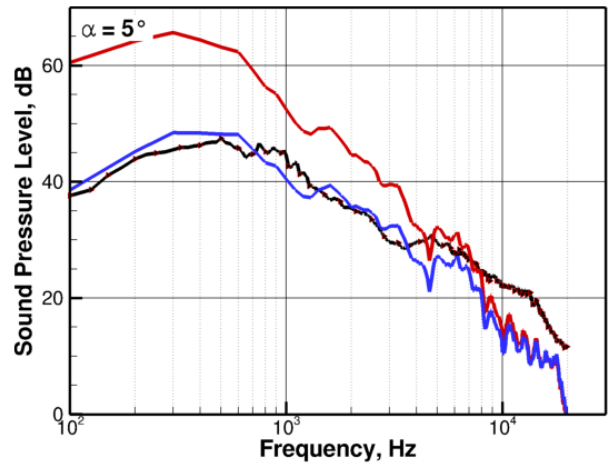(a) Source patch with relaxation parameter σ
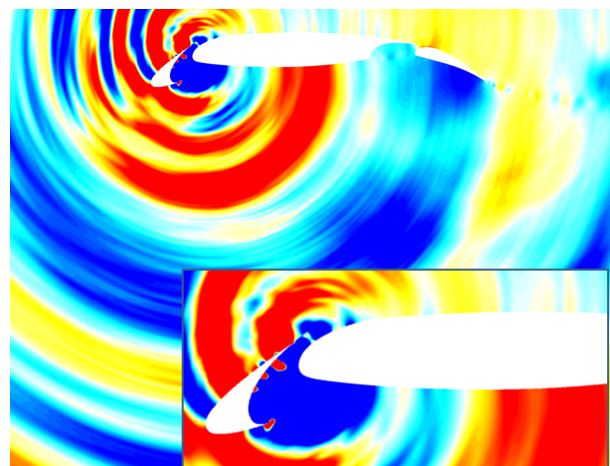
(b) Sound field

**Figure 25. High-lift simulation with relaxation parameter derived from Eq. (65).**

(a) APE+FRPM simulation; DISCO (blue solid line), PIANO (red solid line), DNW measurement (solid black line)
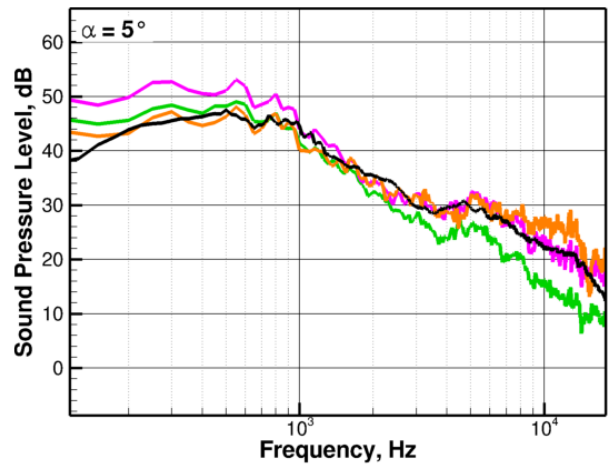
(b) LEE+FRPM, forced eddy simulation, vorticity model B; narrow band spectrum (red solid line), narrow band spectrum + 3dB/octave + off-set (blue solid line)

Figure 26. Narrow band sound spectra for high-lift noise test case.
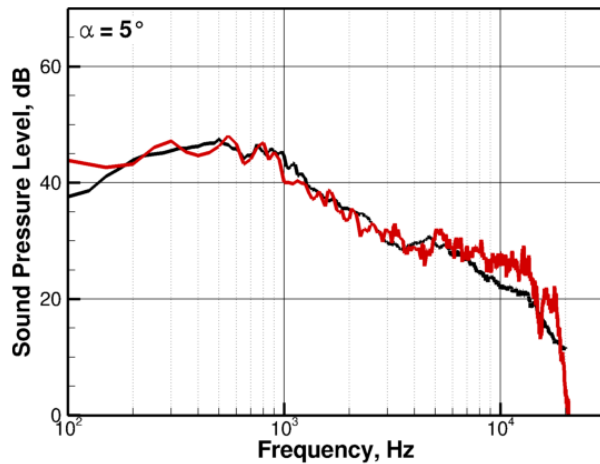
(a) Forced eddy simulation, vorticity model A (red solid line); DNW measurement (solid black line)

(b) Forced eddy simulation, variation of length scale and relaxation parameter; $\sigma = 0.00085$, $l = 0.0085$ (orange line), $\sigma = 0.00125$, $l = 0.0085$ (green line), $\sigma = 0.00125$, $l = 0.0135$ (magenta line)

Figure 27.   CAA simulation versus wind tunnel measurement with eddy relaxation source term, vorticity model A.